Building and Environment 292 (2026) 114283

Contents lists available at ScienceDirect

Building and Environment

journal homepage: www.elsevier.com/locate/buildenv

Evaluation of angular dependence of spectral reflectance and transmittance of glazing systems for improving energy efficiency in buildings

Pablo Santafé-Gabarda [a,*], Jorge Álvarez [a], Adolfo Muñoz [b], M. Mar Barbero-Barrera [c], Joaquín Campos [a], Alejandro Ferrero [a]

[a] Instituto de Óptica "Daza de Valdés", Consejo Superior de Investigaciones Científicas (IO-CSIC), Madrid, 28006, Spain
[b] Universidad de Zaragoza, I3A, Zaragoza, 50018, Spain
[c] Department of Construction and Technology in Architecture, Escuela Técnica Superior de Arquitectura, Universidad Politécnica de Madrid (UPM), Madrid, 28040, Spain

HIGHLIGHTS

- Assuming angle-independent optical properties of glazing limits simulation accuracy.
- Glazing samples are characterized for angular-dependent reflectance and transmittance.
- Measurement guidelines for angular optical properties of glazing are provided.
- A two-parameter model reproduces the angular variation of optical properties.
- PCA reduces data dimensionality and enhances interoperability.

GRAPHICAL ABSTRACT

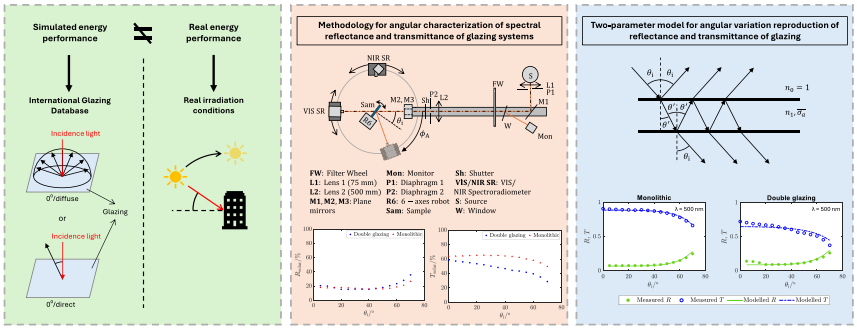

ARTICLE INFO

Dataset link: Database with measurements of reflectance and transmittance of glazing systems and materials for energy efficiency evaluation in buildings (Original data)

Keywords:
Energy efficiency
Fenestration
Glazing
Optical properties
Physics-based model
PCA

ABSTRACT

Dynamic simulation has become an essential tool for energy and daylighting simulations in buildings. However, researchers worldwide highlight the discrepancies between simulated and real performance in buildings. An important limitation is that most databases used in simulation software only include measurements of diffuse reflectance and transmittance of glazing systems with directional-normal incidence. In this work, a methodology for measuring spectral reflectance and transmittance for different angles of incidence of glazing systems has been developed, and the measurements on a broad set of representative samples, for the spectral range 380 nm - 2500 nm with 5 nm resolution and for angles of incidence from 0° to 70° in steps of 5°, have been made publicly available. A simple physics-based model has been proposed, which fits the measurement results with a standard error of the estimate (SSE) below 0.01 in most cases, and a method to apply a principal components analysis (PCA) to the measurement data has been presented, which allows to the amount of data by up reducing 4 times while keeping the relevant information. The results of this work aim to enable more reliable energy simulations to improve the energy efficiency of buildings.

* Corresponding author.
Email address: pablo.santafe@csic.es (P. Santafé-Gabarda).

https://doi.org/10.1016/j.buildenv.2026.114283
Received 9 July 2025; Received in revised form 21 January 2026; Accepted 22 January 2026
Available online 29 January 2026

1. Introduction

1.1. Impact of fenestration systems on the energy demand of buildings

Building is one of the concerning issues related to the route towards decarbonization, as remarked in 2018 by the European Green Deal [1] and supported by different energy efficiency directives towards the nearly-zero energy buildings (NZEB) in the last decades [2]. Indeed, buildings are one of the economic sectors of higher impact, representing almost 27% of the global final energy consumption [3]. According to Eurostat, in 2023, 63.1% of the energy consumed in households in the European Union (EU) was related to space heating and cooling, while lighting and electrical appliances represented 14.5% [4]. Under these circumstances, both thermal conditioning and lighting are the most striking topics in energy consumption in buildings.

Lighting plays an important role in the reduction of energy demand. Although its impact has been considerably reduced in the last decades by the LED technology, in the residential sector half of the lamps are still obsolescent [5], and the penetration of LEDs is still weak in other sectors. The tertiary sector is especially concerning due to its long operating hours and demanding conditions. Commonly between 17% and 40% of the energy consumption is related to lighting in this sector [6,7]. Thus, the optimization of daylight remains a key strategy for reducing energy consumption in buildings.

In the case of thermal conditions, it should be highlighted that 60% of the residential and 44% of the service sector covered floor area in buildings are previous to 1980 [8]. This means that they were built before the first regulations on the thermal performance of buildings. Thus, a huge building stock is inefficient from the thermal point of view and they must be adapted to the new requirements. In this regard, the building envelope takes special relevance since it defines the thermal fluxes between outdoor and indoor spaces [9].

Among the different elements of the envelope, glazing systems, especially windows, represent between 19% and 33% of the thermal loads associated with the building envelopes [10,11]. The optimization of the window systems may allow from 3% to 9% of the energy consumed by buildings to be saved, according to the literature [12–14]. In this regard, a realistic analysis of the envelope performance is essential to forecast the most suitable strategies to reduce energy consumption in the search for zero emission buildings (ZEB) [15–18]. In Spain, the energy saving associated with the fenestration could even increase up to 25% according to the IDAE (*Instituto para la Diversificación y Ahorro de la Energía*) [19], although it could achieve 86% in single-glazed buildings [20]. Under this circumstance, double glazing arises as a necessity to reduce the impact of fenestration in buildings [21]. Indeed, Forughian et al. concluded that thermal loads can be reduced by up to 50% when double-glazing systems are compared to single ones, which implies a reduction of 12.4% in the total energy consumption [22]. This percentage clearly depends on the type of glazing, but also on the window-to-wall ratio [23,24]. Nowadays, different directives require the use of double or even triple glazing to comply with the standards [25].

Since a huge percentage of energy losses in buildings is attributed to the glazing, different research arises in the search for optimal solutions attending to different parameters such as the window-to-wall ratio (WWR) which could imply a reduction of the total energy consumption from 10% in cold areas [26], to 20% in hot areas such as Miami [27] or 23% in Shenyang city [26], which has a humid continental climate. Other authors found that this percentage could increase up to almost 30% [28,29], although the percentage could vary substantially depending on the type of building and location [30,31]. In this line, the evaluation of the indoor daylighting performance, i.e., the combination of artificial lighting and daylighting, could imply savings that achieve up to 61% of energy in Athens or 45% in Stockholm in north-oriented facades [32].

Apart from this, an accurate characterization of the glazing components becomes crucial to enhance energy efficiency in buildings [33]. The incorporation of specific low-emissivity films is an important research line in this topic, with reductions in the annual energy consumption for heating from 3% [34] to 10% [35], although higher percentages of savings could be achieved in cooling depending on the specific characteristics of the location as well as the optical properties of the glazing system [34]. Indeed, optical characterization defines the indoor energy balance through solar radiation [36,37]. Regarding this, smart glazing (or dynamic glazing) could achieve up to 40% of annual energy savings for offices [38]. However, in a previous stage, glazing components clearly define the indoor performance and daylighting, and then window and glazing properties can be optimized for the reduction of energy consumption in buildings [39]. In this regard, energy savings could achieve up to 57% depending on the selection of glazing components [40].

Together with the energy performance, glazing systems determine the daylight factor of buildings, which is the ratio between the illuminance at a given plane due to the light received directly or indirectly from a sky of assumed or known luminance distribution, and the illuminance on a horizontal plane due to an unobstructed hemisphere of this sky, excluding the contribution of the direct sunlight in both cases [41,42]. Daylighting is one of the most important environmental parameters for indoor comfort conditions [43–45] and health promotion [46,47], and it is directly related to mental health [48]. According to some studies, the promotion of daylighting increases productivity and well-being since it improves the synthesis of vitamin D while synchronizing circadian rhythms [49–53]. Furthermore, global electricity consumption in lighting in 2022 was 466.96 TWh in residential and 1268.68 TWh in services [7], with clear differences among countries due to the influence of climate but also to the envelope configuration and the indoor comfort conditions, among others [54–56]. Despite the energy efficiency measures, a general increase in energy consumption in the tertiary sector was observed between 2000 and 2020 [7,57]. Thus, an accurate characterization of the glazing systems is required to optimize the distribution of the indoor daylight and contribute to the improvement of environmental, economic and well-being factors.

1.2. Dynamic simulation of buildings and research gap

The complexity of the high number of parameters to take into account in the design of buildings explains why, in recent years, the dynamic simulation of buildings has become a key tool for designers, architects and engineers. It allows optimal solutions for building envelopes to be predicted and, by extension, enables the most suitable glazing materials and systems to be selected and their performance to be evaluated [58,59]. Many designers, architects and engineers use different energy simulation software such as EnergyPlus™, from DOE (Department of Energy of US), DesignBuilder, which uses the calculation engine of EnergyPlus™ with a more friendly interface, or even others depending on the stage and the scale of the analysis [60]. These software tools can perform both energy and daylighting simulations. In spite of the agreed convenience of building simulations for the optimization of design, worldwide research highlights the discrepancies between those models and the real performance of buildings. These discrepancies can result, for instance, in real energy consumption being up to 2.5 times higher than the predicted performance in some regions [61,62]. In Asia, Zheng et al. identified that the gaps could reach up to 4 times the predicted energy consumption in educational and research buildings [63]. Similarly, Chaturvedi et al. evaluated the effectiveness of energy models in the USA, China and India [64]. In general, standard simulations show larger discrepancies in cooling energy demand than in heating demand [65], which makes them especially relevant considering the current global increase in temperatures. The availability of more detailed information on the relevant materials and methods to be included in the simulations would reduce these discrepancies and, consequently, would notably improve the energy and lighting optimization of buildings.

Although most of the building envelope materials are diffuse or quasi-Lambertian, they can exhibit an optimal reflectance for a specific

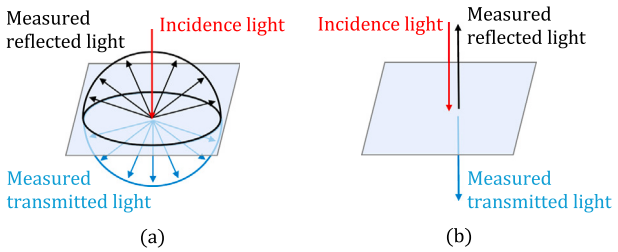

Fig. 1. Diagram of the (a) 0°/diffuse and (b) 0°/direct standard measurement geometries for reflectance and transmittance.

range of angles [66]. In the case of glazing materials and systems, an accurate knowledge of their optical properties (reflectance, transmittance and emittance) depending on the angles of incidence and emission is required. Commonly, analysis for building applications of glazing systems are centered on the performance of glasses attending to the spectral distribution, without consideration of the lighting geometry. For instance, in 2022 Costanzo et al. evaluated the spectral transmittance of colored glazing tiles in situ in the spectral range 350 nm - 1000 nm. In this research, light irradiates the sample using light sources with spectral distributions as illuminants D55 and D65 to simulate real sky conditions but there is no consideration of the angle of incidence and its effect on the transmittance and reflectance, since it is irradiated only in the normal direction [67]. A similar research study was conducted by Sacht et al. in 2021, who evaluated the transmittance of some types of glazing for facades through spectrophotometric characterization in the 200 nm - 1100 nm spectral range only at normal incidence [68].

In the literature, some research about the influence of the angle of incidence on the optical properties of glazing materials can be found, such as the ones developed by Santos & Roriz in 2007 and 2012, where they studied the variation of the visible transmittance and the solar factor, respectively, of different glasses and other transparent materials [69,70]. Another example is found in the work developed by Ghosh et al. in 2014, in which the optical properties of uncoated glass at various incidence angles are compared to those of a glass coated with an effective heat absorbing coating developed by themselves for thermal comfort [71]. These studies highlight the importance of studying the optical properties of glazing materials and systems for different angles of incidence. Nevertheless, with the advent of novel glazing materials, there is now a pressing need for more comprehensive studies focusing on contemporary commercial glazing systems.

Measurements of reflectance and transmittance are usually restricted to specific standard geometries and cannot always be extrapolated to other geometries, such as those for the operative conditions of the glazing systems. Simulation software commonly considers reflectance and transmittance values as independent of the geometry, as collected in the International Glazing Database (IGDB) [72]. This database includes spectral measurements between 300 nm and 2500 nm at 5 nm intervals measured with a geometry 0°/diffuse and/or geometry 0°/direct (see Fig. 1), according to the National Fenestration Rating Council (NFRC) 300 procedure [73]. Therefore, the direction of incidence is always included as normal to the surface and the measurement of the optical properties is diffuse and/or direct, without consideration of other geometries, which are very important in the glazing performance.

1.3. Optical characterization of glazings

According to the International Lighting Vocabulary, reflectance and transmittance are defined as the quotient of reflected, or transmitted, radiant flux and incident radiant flux [74]:

$$R = \frac{\Phi_r}{\Phi_i}, \tag{1}$$

$$T = \frac{\Phi_t}{\Phi_i}, \tag{2}$$

where R stands for reflectance, T for transmittance, Φ_r for the reflected radiant flux, Φ_t for the transmitted radiant flux, and Φ_i for the incident radiant flux. These definitions, however, must be complemented with the specification of the geometries for which the radiant fluxes are evaluated. Reflectance and transmittance depend on the angle of incidence and on the geometrical configuration of the irradiation, which can be diffuse, directional or conical, where the latter includes any intermediate configuration between directional and diffuse [75]. Regarding the reflected (or transmitted) radiant flux, it usually refers to the total reflected (or transmitted) flux, which can be angularly distributed in different ways.

The regular reflection, also known as specular reflection, propagates the radiant flux in a specific and predictable direction (specular direction), and so does the regular transmission. In these situations, the evaluation of reflectance and transmittance can be done by evaluating these quantities at the pertinent direction depending on the irradiation direction. However, when the reflection and the transmission are not purely regular and the diffuse component is not negligible, the total reflected (or transmitted) radiant flux propagates in all directions. In that case, the diffuse reflectance (or transmittance) can be measured, but that does not provide any information on the angular distribution of the reflected (or transmitted) radiant flux.

The Bidirectional Reflectance Distribution Function (BRDF) allows the reflectance at any pair of incidence and collection directions to be described. The BRDF was defined by Nicodemus et al. in 1977 [76] as the distribution function of the bidirectional radiance coefficient, which is the ratio between the elementary radiance of a surface, $\mathrm{d}L_r$, and the received elementary irradiance on that surface, $\mathrm{d}E_i$, for specific irradiation and collection directions, $\mathbf{r}_i$ and $\mathbf{r}_r$, respectively:

$$f_r(\mathbf{r}_i, \mathbf{r}_r) = \frac{\mathrm{d}L_r(\mathbf{r}_r)}{\mathrm{d}E_i(\mathbf{r}_i)}. \tag{3}$$

Similarly, the Bidirectional Transmittance Distribution Function (BTDF) allows one to characterize the transmittance at any geometry. It is defined as the ratio between the elementary radiance of the back surface of a sample, $\mathrm{d}L_t$, and the received elementary irradiance on the front surface of that sample, $\mathrm{d}E_i$, for specific irradiation and collection directions, $\mathbf{r}_i$ and $\mathbf{r}_t$, respectively:

$$f_t(\mathbf{r}_i, \mathbf{r}_t) = \frac{\mathrm{d}L_t(\mathbf{r}_t)}{\mathrm{d}E_i(\mathbf{r}_i)}. \tag{4}$$

Whereas the BRDF applies to describe the reflective properties of the surface with respect to the incidence and reflection directions, the BTDF similarly addresses the transmissive properties. Both functions can be reduced to a more general one known as the Bidirectional Scattering Distribution Function (BSDF), which assumes negligible volume-scattering. Nowadays, very sophisticated measuring systems, called goniospectrophotometers, are able to provide traceable measurements of the BRDF, the BTDF, and the BSDF and are available in national metrology institutes (NMIs) and other research centers [77–82]. One of them [78] was used for the measurements presented in this article. These distribution functions represent the relevant quantities to characterize samples whose reflectance (or transmittance) is completely dominated by the diffuse component, while the reflectance (or transmittance) coefficient is the relevant quantity to characterize samples whose reflectance (or transmittance) is completely dominated by the regular component. In some cases, a sample can have a notable amount of both components (such as tinted glasses or dome daylighting films). In those cases, both quantities need to be evaluated to characterize the dependence on the incidence angle for both the regular and the diffuse components.

The inclusion of BRDF and BTDF, and the regular reflectances and transmittances for different angles of incidence, in the dynamic simulation of buildings, and on the international and national databases of

glazing, would allow a detailed analysis of the performance of glazing systems considering the variation of the inclination of solar rays, and consequently as a function of the time of the day, season or latitude. But also, it would allow an accurate simulation of the energy performance of buildings in terms of heat gains for winter conditions or even the solar protections under summer ones. This information is very important in the design of the envelopes, mainly windows and curtain walls, as was concluded in the research about the effect of the inclination of glasses performed by Arici et al. a few years ago [83]. Nowadays, there is an ongoing effort on the standardization of the characterization of angle-dependent transmittance and reflectance properties of complex fenestration systems (CFS) and the generation of BSDF data sets from measured or simulated data for use as input to simulation tools [84]. Besides, the International Energy Agency has developed a task on integrated solutions for daylighting and electric lighting in which BSDF characterization of daylighting systems has played an important role [85]. Several measuring systems and methods for BSDF data acquisition have been used. Most of them are able to measure the reflectance and transmittance at any angle of incidence and detection, but only one of them can provide spectral resolution to the measurements [86]. In this work, a similar measuring system is presented, which allows BSDF measurements at different in-plane geometries, including different incidence and detection angles, with spectral resolution.

1.4. Available models for reflectance and transmittance of glazings

Analytical and empirical models have been proposed over the last two decades to predict the dependence of the reflectance and the transmittance on the angle of incidence [87–90]. The measurements provided in this article will allow adequate models to be tested and selected for use in simulations. Different researchers have developed studies in the years regarding recent design of building envelopes by dynamic building simulation in terms of energy performance or daylighting. These are combined with statistical analysis to reduce the number of parameters or even to optimize the parameters with higher influence on the energy simulation of buildings [17,91]. The Design of Experiments method, Analysis of Variance test and their combination with other statistical tests [92,93] are commonly used. Additionally, experimental tests are usually performed regarding aspects such as the geometry of the windows, shading devices, glazing properties or types of glasses [20,94–96]; or the analysis of specific layers or their mineralogical composition [97–100]. However, most of the research has focused on one type of glass, combination or film, without a comparison among them and, above all, a deep characterization in which the influence of the angle of incidence/measurement despite the optical properties is not considered, in its importance in terms of both energy efficiency and daylighting. In this work, the monolithic model presented by Rubin et al. [101] has been used to fit the measurements. This model assumes a single symmetrical layer and applies the Fresnel equations to obtain the refractive index and the extinction coefficient of the material only by measuring its transmittance and its reflectance, which is assumed to be equal from both sides. This model is very useful for any unknown dielectric material and its performance in the simulation of solar transmittance and reflectance (at least from one side) was compared with that from a detailed model, showing discrepancies at an incidence angle of 60° around or even below 1% for simple-structure materials, such as transition metal coatings, and up to 5% for more complex materials [87].

1.5. Objective of this work

The objective of this work is to establish a framework for considering the dependence of the incidence angle at the glazing materials and systems on the assessment of energy efficiency in buildings. This methodology consists of:

1. A well-defined measurement method, where the important methodological issues are identified. These issues are explained in this paper and possible solutions are proposed.
2. A deep spectrophotometric characterization of relevant representative contemporary glazing materials and systems, with the measurement of reflectance and transmittance at different angles of incidence, thus, updating the already existing studies and broadening the recent studies on the characterization of new glazing materials only at normal incidence. In this way, a selection of different types of glasses together with their combinations in terms of double glazing, type of air/argon chamber in insulating glass units (IGUs), use of butyl for laminated glasses, or solid thin films to improve solar control or reduce the emittance of glasses, was made.
3. Share of the obtained measurement data in a public repository for general use by the scientific community [102].
4. The proposal of a physical model able to predict the dependence of the reflectance and transmittance of the glazing systems on the incidence angle with a very low number of parameters obtainable from measurement using a low number of geometries, and the proposal of a method based on principal components analysis (PCA) to reduce the data while keeping the relevant information. Both proposals, alone or in combination, should be important for including the measurement data in current software simulations.

2. Description of the evaluated glazing samples

Advances in thin-film deposition technologies for coating insulating glass have made energy-efficient windows both affordable and commonplace in contemporary construction. In this study, a stock of glazing samples was collected from three of the world's leading glass manufacturers. The collection comprises 66 samples: 29 monolithic glasses, 10 laminated glasses and 27 IGU (25 single-chamber units and 2 double-chamber units). These samples have different sizes and thicknesses. The classification of the samples is shown in Table 1 together with the identifiers for manufacturers, ID_M, and physical specimens, ID_S, the latter being a non-descriptive internal identifier. Hereafter, each sample is denoted as ID_M-ID_S. A diagram of the three different types of glazing samples considered in this work is shown in Fig. 2.

2.1. Monolithic glass

Monolithic or float glass is a transparent or translucent material consisting of a single homogeneous sheet of glass, produced through manufacturing processes such as float glass production [103]. This type of glass is characterized by its continuous structure, which provides uniform optical properties, as well as controlled mechanical properties within its specific limits. Its use is widespread in architectural applications, where it is used as a base for subsequent treatments or

Table 1
Structural description of the collected glazing samples, together with their identifiers. Each sample is denoted in this paper as ID_M-ID_S.

ID_M	ID_S	Type	Dimensions (cm × cm)	Thickness (mm)
M1	01–07 13–25, 27, 29, 31	Monolithic	20 × 30	6
			10 × 10	4–12
	26, 28, 30, 32–34	Laminated	10 × 10	4–12
	08–12	IGU	20 × 30	26
M2	01–12	IGU	20 × 30	26
M3	01–04	Monolithic	10 × 10	4–6
	14,15		20 × 20	
	05–08	Laminated	10 × 10	8–12
	09–12	IGU	20 × 20	24–26
	16–19			
	13, 20	IGU (triple)	20 × 30	41–44

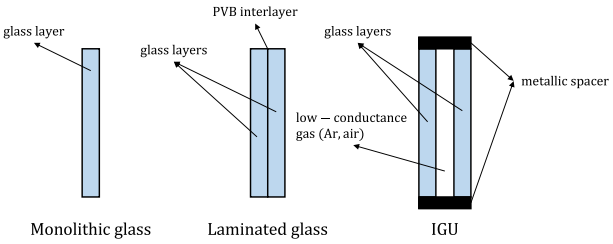

Fig. 2. Diagram of the three different types of glazing samples considered in this work.

combinations with other elements, such as coatings, or formal modifications such as a combination of glasses for systems or lamination. All the specimens in our study feature a solar control coating deposited on one of their surfaces and are available in various sizes, see Table 1.

2.2. Laminated glass

A small part of the glazing stock of this study consists in laminated glass, which is composed of two glass panels bonded together by a polyvinyl butyral (PVB) interlayer. The specimens are available in both transparent and translucent forms.

2.3. IGU

To minimize thermal losses due to heat transfer by radiation and conduction mechanisms, an IGU is manufactured by placing two (double glazing) or even three (triple glazing) glass panels with parallel flat surfaces, separated by a metallic spacer filled with an absorbent and an adhesive to bond the glass to the spacer. To reduce thermal transfer by convection through the IGU, a low-conductance gas, typically argon, is used to fill the gap. Argon has a larger molecular size compared to nitrogen and oxygen (air).

All specimens feature a solar control coating deposited on the inner surface of the glass facing the exterior, in contact with the argon-filled cavity to increase its durability. Most of the double-glazing IGUs are filled with a 9:1 mixture ratio of argon and air, respectively, while only a few of them are filled solely with air. Some specimens also exhibit a slight coloration and/or translucency.

3. Measurements

3.1. Measuring system

The measuring system used in this work is based on an automatic goniospectrophotometer, which has been previously described in the literature [78]. This system was originally designed for BRDF measurements in the visible range. For this work, it was modified in order to allow measurements of transmittance and to cover the near-infrared spectral range, up to 2500 nm.

It comprises three subsystems: the lighting system, which is fixed and includes a broadband Xe lamp and an optical system that directs the irradiation beam towards the sample; the positioning system, which consists of a 6-axis robot arm that can orient the samples in several directions relative to the irradiation beam; and the detection system, which comprises two different spectroradiometers (one for the visible range and the other for the near-infrared range) that are placed on two movable platforms that can rotate around the sample along a circular track. A diagram of the measuring system is shown in Fig. 3(b).

The lighting system is composed of a broadband Xe lamp (Hamamatsu Super-Quiet Xenon Lamp, model: L2175 150 W) and a Köhler optical system (lens L1 and L2 with focal lengths of 75 mm and 500 mm, respectively) that produces a uniform irradiation on the sample surface. After the first lens, a diaphragm (P1) allows the adjustment of the irradiation size on the sample surface. A second diaphragm

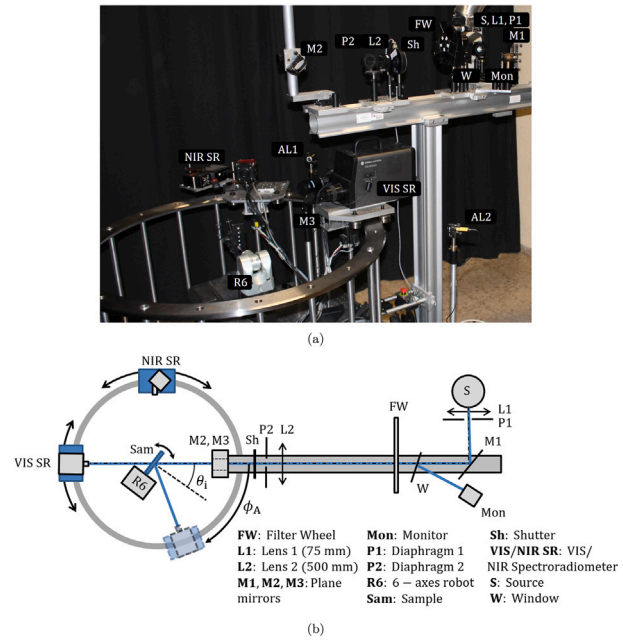

Fig. 3. Photograph (a) and picture (b) of the measuring system.

(P2) placed after the second lens allows the irradiance on the sample surface to be controlled. Additionally, a filter wheel (FW) with different neutral density filters allows different levels of attenuation to avoid the saturation of the response of the detection device. An uncoated fused silica plate (W) redirects approximately 8% of the incident radiant flux towards a photodiode (Mon), which monitors the source signal (two photodiodes are available: a Si photodiode for the visible range and an InGaAs photodiode for the NIR range). After the Köhler system, two plane mirrors (M2 and M3) oriented at −45° and 45°, respectively, from the optical axis form a periscopic arrangement that can allow retroreflection measurements when M3 is replaced by a beamsplitter.

The positioning and orientation of the samples are achieved by a 6-axis robot arm (R6). The use of a robot for sample positioning enables placing the center of the sample's surface at the center of rotation of the detection system with negligible uncertainty compared to other sources. For large glazing samples measured in this study, mechanical mounts had to be designed to accommodate different sizes and thicknesses, and only in-plane measurement geometries could be configured.

The detection system includes two detection instruments: a Konica-Minolta® CS-2000 spectroradiometer (VIS SR) for the visible range (from 380 nm to 780 nm), and an Ocean Insight® NIRQuest spectroradiometer (NIR SR) for the near-infrared range (from 900 nm to 2500 nm). However, due to the operational limitations of the two detectors, there remains a 120 nm gap (from 780 nm to 900 nm) within which data cannot be obtained. Both instruments are mounted on two platforms that move along the circular track around the sample. Each platform moves independently, and they cannot be operated simultaneously due to mechanical limitations of the system. Thus, a separate measurement is performed for each spectral range.

3.2. General considerations of the measurement process

In the measurement process, radiation impinges on the surface assumed to be placed towards the exterior of the building. The samples were located sequentially at the different geometries to be evaluated, and acquisitions were taken with the spectroradiometers, in signal and dark conditions. The acquisitions were dark-subtracted, corrected for light source instabilities using the monitor signal, and for photoresponse nonlinearity of the detectors. The corrected acquisitions with the sample

are divided by the corrected acquisitions of the reference. As explained in Sections 3.3 and 3.4, the reference for transparent glazing samples is the incident beam, while for diffuse glazing samples it is a diffuse reflectance standard.

Generally, the surface of the sample aligned in the center of the goniospectrophotometer is the closest to the spectroradiometers, i.e., the interior surface in reflectance measurements and the exterior surface in transmittance measurements. However, for diffuse glazing samples, the surface aligned in the center was the diffuse surface of the sample. The measurement area is determined by the field-of-view of the spectroradiometers, which are always focused on the center of the goniospectrophotometer, and it is always over-irradiated by the large (6 cm in diameter) and uniform irradiation beam. This means that the response of the spectroradiometers is directly proportional to the radiance of the sample surface. The origin of the reference system for sample rotation is always defined at the center of the goniospectrophotometer.

The spectral distribution of the irradiation beam is provided by the Xe lamp, whose spectral irradiance can be found in the manufacturer's specification sheet [104]. The angular resolution on the irradiation depends of the aperture of diaphragm P2, which controls the irradiance on the sample by adjusting the irradiation solid angle. For the measurements presented in this work, an intermediate aperture of the diaphragm was used, in order to achieve a compromise between the amount of light available for the measurement and the angular resolution, which resulted in approximately 0.5° approximately. The VIS spectroradiometer features a wavelength resolution of 1 nm, with a 5 nm bandwidth, and an angular resolution of 2.5°, as stated in Ref. [78]. On the other hand, the NIR spectroradiometer features different wavelength resolutions depending on the slit size [105]. In the measurements of this work, a high spectral resolution was not required since the evaluated samples smooth reflectance and transmittance spectral distributions. Thus, the largest available slit size was used to improve the signal-to-noise ratio (SNR), which resulted in a full width at half maximum (FWHM) of 26 nm, approximately. Its angular resolution was determined by the macro lens attached to it, which collects all the light within an apex angle of 2° approximately.

The relative expanded uncertainty of the measurements, depicting 95% confidence intervals, ranges from 1% to 7%, depending on the SNR of the corresponding measurement. It can reach values slightly over 10% in those very specific cases where either the reflectance or the transmittance of the glazing sample is very low. The specific values of the standard uncertainty are available together with the measurement data in the public repository of Ref. [102]. All the measuring instruments have been previously characterized and calibrated. The main uncertainty sources arise from the signal-to-noise ratio of the detection devices and the correction factor for the instability of the light source in the case of the measurements on non-diffuse glazing samples. In the case of diffuse glazing samples, the uncertainty mainly depends on the uncertainty of the calibrated BRDF value of the white standard diffuser [78].

Other aspects not considered in this work can affect the measurement uncertainty, such as the non-uniformity of the irradiation beam, the uneven state of the sample to be measured, or even some environmental factors. However, the influence of these aspects depends on the measured quantity itself and, thus, it is very difficult to account for it in the uncertainty budget without studying them in advance. Instead, they are controlled in order to minimize their effect in the measurement, for instance by using a very uniform irradiation beam or selecting high-quality samples that ensure uniformity of their surface. Besides, some control measures are taken in the laboratory, such as the use of gloves for holding the samples or the accurate alignment method that ensures a perpendicular orientation of the sample surface with respect to the incident beam. On the other hand, both the temperature and relative humidity are monitored by a probe and controlled through an air conditioner installed in the laboratory, which maintains a room temperature of 23 °C ± 2 °C and a relative humidity below 50%. In this regard, no correlation has been observed between the measurement results and the slight variations of the environmental conditions in the laboratory.

3.3. Measurement of non-diffuse glazing samples

Non-diffuse glazing samples are those for which the reflected or transmitted light that propagates in a direction different from the regular direction (specular or refraction directions, respectively) can be considered negligible. Thus, the measurement of this kind of sample consists of evaluating the ratio of the incident radiant flux on the sample surface and the reflected or transmitted radiant flux in the regular direction, which also corresponds to the ratio of radiances when the measurement conditions are the same. In this way, the measurement equations used for reflectance, R, and transmittance, T, become:

$$R = \frac{L_r}{L_i} = \frac{S_r}{S_i} F_\tau F_{mon}, \tag{5}$$

$$T = \frac{L_t}{L_i} = \frac{S_t}{S_i} F_\tau F_{mon}, \tag{6}$$

where L_r and L_t denote the reflected and transmitted radiance, respectively, and L_i the incident irradiance. S_r, S_t and S_i are the obtained signals from the acquisitions of the reflected, transmitted and incident beams, respectively, in the corresponding spectroradiometer (all dark-subtracted and corrected for non-linearity), F_τ is a correction factor accounting for the ratio of the transmittances of the different neutral-density filters from the filter wheel (FW) used in each acquisition, and F_{mon} is a correction factor accounting for the ratio of the signal registered by the photodiode (Mon) monitoring the light source stability in each acquisition (see Section 3.1). The transmittances of the neutral-density filters have been previously characterized in the laboratory while the registered signal by the photodiode is averaged from 10 repetitions to obtain a corresponding uncertainty from the standard deviation of the average. Both registered signals, $S_{r,t}$ and S_i, and the non-stability correction factor, F_{mon}, are the main uncertainty sources of this kind of measurement.

The evaluation of the incident radiance is performed by moving the sample out of the beam path and driving the platform of the corresponding spectroradiometer to the position of normal incidence, i.e., $\phi_A = 180°$ (see Fig. 3(b)). The incident radiance is determined by the radiant flux collected by the spectroradiometer in this configuration, within the measurement area and its collection aperture.

The reflected and transmitted radiant fluxes are evaluated under exactly the same configuration of the spectroradiometer, but once the surface of the samples are located at the measurement plane. Thus, the ratio of registered signals equals the ratio of radiances. The sample is sequentially orientated at different angles with respect to the irradiation beam and the reflected, or transmitted, radiant flux is acquired at the corresponding regular direction. In this work, the measurements were performed for 15 different angles, from 0° to 70° in steps of 5°, although in the case of reflectance no value was obtained at 0° due to the obstruction of the irradiation beam. It must be noticed here that measuring at large angles of incidence, which has some important methodological issues, is very important for realistic evaluations. High angles of incidence are very common on vertical surfaces at low and intermediate latitudes, at those times when the solar elevation angle is maximum. A complete measurement of either the reflectance or the transmittance of one sample took no more than 6 min.

The measurement approach presented in this work satisfies Eqs. (1) and (2). However, not all the incident flux is collected by the detector but only a part of it, that within the same solid angle for which the incident radiant flux is evaluated. This approach is possible only if: (1) the incidence beam uniformly over-irradiates the collection area, and (2) the diffuse component of reflectance and transmittance is negligible (the reflected or transmitted radiant flux through the solid angle is not attenuated by scattering out of the regular direction) [106]. This

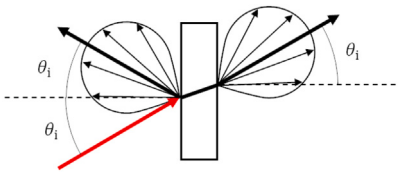

Fig. 4. Diagram of a general angular distribution of the reflected and transmitted radiant flux by a diffuse glazing sample. The thick red arrow indicates the irradiation direction and the thick black arrows the regular direction for both the reflected and transmitted radiant flux. (For interpretation of the references to colour in this figure legend, the reader is referred to the web version of this article.)

hypothesis cannot be stated with diffuse samples, since in that case the attenuation is also due to diffuse reflectance and transmittance, which yield reflected and transmitted radiant flux out of the regular directions, and consequently are not collected by the spectroradiometers in that measurement condition (see Section 3.4).

3.4. Measurement of diffuse glazing samples

In the case of diffuse glazing samples, the reflected or transmitted light in those directions different from the regular direction is not negligible (see Fig. 4). In such cases, the International Commission on Illumination (CIE) recommends measuring reflectance and transmittance with an integrating sphere that integrates the reflected or transmitted radiant flux in any direction [107]. However, for more detailed information on the scattering at different incidence and collection directions, the BRDF and BTDF must be measured, as explained in Section 1. This is the approach followed in this study.

The measurement procedure for this kind of glazing samples is similar to that used for the measurement of non-diffuse glazing samples, but in these cases the acquisition of the incident radiant flux is replaced by the acquisition of the radiance of the surface of a diffuse reflectance standard for which its BRDF value at 0° irradiation and 45° collection is known. This procedure allows for the calculation of the incident irradiance in an indirect way, assuming constant measurement conditions. The BRDF or the BTDF are calculated as:

$$f_s(\mathbf{r}_i, \mathbf{r}_s) = \frac{L_s(\mathbf{r}_i, \mathbf{r}_s)}{E_i(\mathbf{r}_i)} = \frac{f_{s,ref} L_s(\mathbf{r}_i, \mathbf{r}_s)}{\cos\theta_i L_{s,ref}}, \tag{7}$$

where $f_{s,ref}$ denotes the BRDF value of the diffuse reflectance standard at the reference geometry (0° : 45°), $L_{s,ref}$ denotes the measured radiance of the diffuse reflectance standard at the reference geometry, and $L_s(\mathbf{r}_i, \mathbf{r}_s)$ is the measured radiance of the glazing sample at any other geometry, with $\mathbf{r}_i$ being the irradiation direction, which is defined by the angle of incidence θ_i, and $\mathbf{r}_s$ being the collection direction, defined by the collection angle θ_r. Note that the key idea of this approach is to express the incident irradiance in terms of the known value of the BRDF of a diffuse reflectance standard, since it only varies through the cosine of the incident polar angle of the specific measurement geometry.

Eq. (7) can be rearranged in terms of the registered signals by the corresponding spectroradiometer, resulting in the following measurement equation:

$$f_s(\mathbf{r}_i, \mathbf{r}_a) = \frac{f_{s,ref} S_s(\mathbf{r}_i, \mathbf{r}_s)}{\cos\theta_i S_{s,ref}} F_\tau F_{mon}, \tag{8}$$

where $S_s(\mathbf{r}_i, \mathbf{r}_s)$ and $S_{s,ref}$ are the obtained signals from the collected radiance of the evaluated sample at the specific geometry and the diffuse reflectance standard at the reference geometry, respectively, in the corresponding spectroradiometer (dark-subtracted and corrected for non-linearity), and F_τ and F_{mon} are the correction factors of the transmittance for the used neutral-density filters and the non-stability of the light source as defined in Section 3.3. In this case, the main uncertainty sources are the registered signals, S_s and $S_{s,ref}$, in the corresponding spectroradiometer and the BRDF value of the diffuse reflectance standard, $f_{s,ref}$, whose uncertainty arises from the calibration performed in the laboratory. The reproducibility of the measuring system has been proven several times in recent years through intercomparisons with European National Metrology Institutes (NMIs) [108,109].

The acquisition of the radiance of the diffuse reflectance standard at the reference geometry is performed at least once each day or each time the measuring devices are turned off or the measurement conditions change. Then, each diffuse glazing sample is irradiated at 5 different irradiation angles (from 0° to 60° in steps of 15°), and the spectral reflected or transmitted radiance is collected at 10 different equispaced in-plane collection angles from the normal of the surface (from 8° to 68° in steps of 15°) for each irradiation angle, which results in 50 different measurement geometries for each sample and each measured quantity (BRDF or BTDF). These kinds of measurements need around 13 min to be completed.

In these cases, the angular resolution of the measurement is determined by the collection solid angle of the corresponding spectroradiometer, which is narrow enough to assume that the angular distribution of the reflected or transmitted radiance collected within it is uniform. This assumption is only valid if no peaks in the angular distribution of either the reflectance or the transmittance are observed. The diffuse glazing samples evaluated in this work present the diffuse surface in one of their interlayers, so that the first surface is always smooth. Thus, these samples also present a contribution of regular reflectance from their first surface, apart from the diffuse reflectance generated in the diffuse interlayer. In order to fully characterize these samples, their regular reflectance has also been measured in both visible and NIR spectral ranges according to the measurement procedure described in Section 3.3.

3.5. Methodological issues

In the process of measuring the reflectance and transmittance of glazing systems at different angles of incidence, some methodological issues, mainly in double and triple glazing samples, have been identified: (1) lateral displacement of inter-reflections in both reflectance and transmittance measurements, (2) lateral displacement of the transmitted beam, and (3) partial occlusion of the incident beam due to the rotation of the sample in transmittance measurements.

1. When a collimated beam irradiates the surface of a plane-parallel plate, or a system composed of parallel plates, inter-reflections produce an indefinite number of reflected and transmitted beams. These secondary beams are displaced laterally with respect to the irradiation beam, and this displacement increases with the number of inter-reflections, the thickness of the plate (or the separation between the different plates) and the angle of incidence. In the case of monolithic glazing samples, the thickness is small in comparison with the width of the irradiation beam; thus, the separation of the different reflected and transmitted beams is not relevant because all observed secondary beams are under the same acquisition conditions. However, in the case of IGU samples, where two or three plane-parallel plates are mounted in parallel with a gap between them, this separation becomes significant for high angles of incidence, causing a variation in the acquisition conditions for the different beams, and the consequent measurement error. This effect is shown visually in Fig. 5(a), where secondary beams from the inter-reflections within a double-glazing IGU in reflectance measurement conditions are clearly visible, not being collected by the detector at all. This effect is minimized by using a larger irradiation area, which is limited by the maximum aperture of diaphragm P1 (see Fig. 3). Thus, even using the maximum available irradiation area, this issue might prevent the correct characterization of the reflectance or the transmittance of such glazing samples for

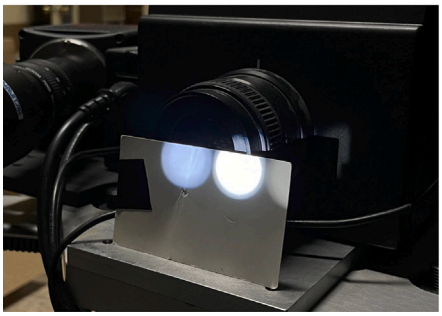

(a) Picture of the inter-reflection produced by a double-glazing IGU irradiated with a high angle of incidence, at the detector position.

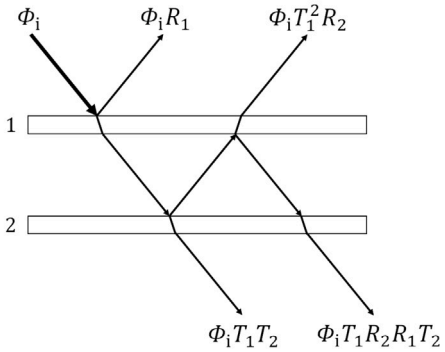

(b) Diagram showing the expected radiant flux of secondary beams in double-glazing IGUs. In this diagram Φ_i refers to the incident radiant flux, and R_1, R_2, T_1 and T_2 refer to the reflectance and the transmittance of the corresponding glass layer (1 or 2).

Fig. 5. (a) Picture and (b) diagram of the beam separation issue in double-glazing systems with separated glass layers.

high angles of incidence. The impact of this potential error depends on the reflectance and transmittance of the different glasses forming the IGU (see Fig. 5(b)). In transmittance measurements, secondary beams are always less intense than the main one, while in reflectance measurements it depends on the ratio $R_1/(T_1^2 R_2)$, with the impact of the error being larger if the ratio is lower.

2. In transmittance measurements, the regularly transmitted beam is laterally displaced due to refraction. This lateral displacement increases with the thickness of the layer and the angle of incidence. In the case of IGU samples, it does not depend on the separation between the different layers. This effect results in different collection conditions of the transmitted radiant flux for each angle of incidence. Thus, a large and uniform irradiation beam is required to avoid this error source, allowing the acquisition conditions to remain constant.
3. Also in transmittance measurements, the occlusion of the irradiation spot by the edge of the sample itself entails a measurement error for very large angles of incidence and thick samples, such as IGUs, since the samples rotate around their back surface in this case. It is a geometrical restriction due to the finite size of the sample and the width of the irradiation beam. Thus, the width of the irradiation beam must be selected according to a compromise that takes into account the issues described above and the edge occlusion for high angles of incidence. In this work, no measurements for angles of incidence higher than 70° were performed due to the edge occlusion.

4. Data analysis and modeling

The measurements are traceable to the International System of Units (SI) through optical standards and procedures and can be arranged in a dataset. These data can be reduced while keeping the relevant information by using empirical or analytical models. A simple model able to predict the variation of the reflectance and transmittance with respect to the angle of incidence would allow a practical use of this kind of measurements in simulation software for evaluating the impact of the different glazing systems on the energy efficiency of buildings. The lower number of parameters required by the model, the fewer measurement geometries would be necessary for determining them.

In the case of non-diffuse glazing samples, where regular reflectance and transmittance are dominant, an analytical model is more feasible than for diffuse glazing materials, where more complex models are required. A simple analytical model for non-diffuse glazing samples has been proposed in this work and it is described in section 4.1.

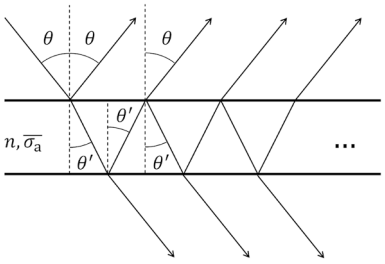

Fig. 6. Diagram of the glazing sample modeled as a dielectric layer with refractive index n and normalized absorption coefficient $\overline{\sigma_a}$. Its thickness t is embedded into the normalized absorption coefficient.

In addition, a principal components analysis (PCA) was applied to the data in order to examine the spectral variation of the reflectance and the transmittance with respect to the geometry. This analysis allows possible errors or special cases to be identified, such as measurement geometries whose spectral content is very weakly correlated with the rest of the geometries. It also allows reducing the dimensionality of the data and, thus, the computational cost. This is discussed in section 4.2.

4.1. Model

The monolithic model from Rubin et al. [101] is used in this work. It is based on the physics of a single dielectric thin layer with refractive index n and absorption coefficient σ_a (see Fig. 6). According to Beer–Lambert's law, the radiance L decreases exponentially with respect to distance d as $L(d) = L(0)\, e^{-\sigma_a d}$. The interactions on both boundaries of this layer are governed by Fresnel equations [110], which for outside/inside refractive indices n_1 and n_2, respectively, yield reflectance $F_r(n_1, n_2, \theta)$ and transmittance $F_t(n_1, n_2, \theta) = 1 - F_r(n_1, n_2, \theta)$ at incident angle θ. The external medium has a refractive index of 1, so external reflectance/transmittance uses $n_1 = 1$, $n_2 = n$, while internal uses $n_1 = n$, $n_2 = 1$; the propagation angle θ' inside the layer follows Snell's law: $\theta' = \sin^{-1}\left(\frac{\sin\theta}{n}\right)$. Under this configuration, light travels a distance $d = \frac{t}{\cos\theta'}$ within layer thickness t, so radiance becomes $L(d) = L(0)\, e^{-\sigma_a t/\cos\theta'}$. Thickness t and absorption σ_a combine into normalized absorption $\overline{\sigma_a} =$

$\sigma_a t$, reducing parameters—this is the principal modification from Rubin et al.

This configuration generates a repeatable geometrical pattern that produces a sequence of reflectance and transmittance interactions at regular intervals. It is assumed that all (infinite) interactions are captured by the sensor, which might not always be the case, so the model calculates reflectance $R\left(n,\overline{\sigma_a},\right)\theta$ and transmittance $T\left(n,\overline{\sigma_a},\right)\theta$ as:

$$R\left(n,\overline{\sigma_a},\theta\right) = F_r\left(1,n,\theta\right) + \sum_{i=1}^{\infty} F_t\left(1,n,\theta\right) e^{-\frac{2i\overline{\sigma_a}}{\cos\theta'}} \left[F_r\left(n,1,\theta'\right)\right]^{2i+1} F_t\left(n,1,\theta'\right)$$
$$= F_r\left(1,n,\theta\right) + \frac{F_t\left(1,n,\theta\right) F_r\left(n,1,\theta'\right) F_t\left(n,1,\theta'\right)}{1-\left[F_r\left(n,1,\theta'\right)\right]^2 e^{-\frac{2\overline{\sigma_a}}{\cos\theta'}}}, \quad (9)$$

$$T\left(n,\overline{\sigma_a},\theta\right) = \sum_{i=0}^{\infty} F_t\left(1,n,\theta\right) \left(e^{-\frac{(2i+1)\overline{\sigma_a}}{\cos\theta'}}\right)^{2i+1} \left[F_r\left(n,1,\theta'\right)\right]^{2i} F_t\left(n,1,\theta'\right)$$
$$= \frac{F_t\left(1,n,\theta\right) e^{-\frac{\overline{\sigma_a}}{\cos\theta'}} F_t\left(n,1,\theta'\right)}{1-\left[F_r\left(n,1,\theta'\right)\right]^2 e^{-\frac{2\overline{\sigma_a}}{\cos\theta'}}}. \quad (10)$$

As shown, this model depends only on two parameters (n and $\overline{\sigma_a}$) per wavelength which account for both reflectance and transmittance.

For a set of reflectance and transmittance measurements ($\hat{R}_{\theta_i}$ and $\hat{T}_{\theta_i}$) at specific angles of incidence, θ_i, the model is adjusted to those measurements. This becomes an optimization problem as:

$$\min_{n,\overline{\sigma_a}} \left(\sum_{\theta_i \in M_R} \left[R\left(n,\overline{\sigma_a},\right)\theta_i - \hat{R}_{\theta_i}\right]^2 + \sum_{\theta_i \in M_T} \left[T\left(n,\overline{\sigma_a},\right)\theta_i - \hat{T}_{\theta_i}\right]^2 \right), \quad (11)$$

where M_R and M_T are the numbers of measurement geometries for reflectance and transmittance, respectively. The model, represented by Eqs. (9) and 10, is fully differentiable, so a gradient descent approach is chosen to solve the minimization problem in Eq. (11). In practice, the minimization problem is implemented with Mitsuba3 [111], a differentiable renderer that provides expressions for Fresnel equations and automatic differentiation. Then, the Adam solver [112] is used to obtain the parameters n and $\overline{\sigma_a}$ that better approximate the measurements.

The obtained refractive index or the normalized absorption coefficient does not represent physical parameters of the glazing sample. Therefore, the parameters of the model are denoted as "effective" refractive index (n) and "effective" normalized absorption coefficient ($\overline{\sigma_a}$). The advantage of this model with respect to purely heuristic models is that it is physically inspired, and as such requires only two parameters for modeling the angular dependence of both the reflectance and transmittance.

The structure of the physical glazing sample and its configuration for measurement might differ from the hypothesis of the model. For instance, the glazing sample might present several layers such as solar coating on top of glass, multiple stacked glass layers, or even air layers as is the case with the IGUs. The model assumes that any combination of layers can be reduced to a single layer with an effective refractive index n and an effective normalized absorption coefficient $\overline{\sigma_a}$. This assumption is always valid for a specific wavelength if the different layers only present regular scattering (or diffuse scattering can be considered negligible). Thus, the main limitation of the model is that the obtained parameters only describe the optical properties of the sample for a specific wavelength and do not characterize their spectral distribution.

In the specific case of IGU samples, discrepancies between the model and the measurement data are expected, since the model assumes that all the internal interactions (inter-reflections) are captured by the sensor and that is not fulfilled when measuring such samples at high angles of incidence, as mentioned in Section 3.5.

4.2. Principal components analysis

Principal components analysis (PCA) is a powerful mathematical technique to identify the different contributions to the variance of multidimensional data. In this work, the adequacy of PCA to synthesize the spectral variation of the reflectance and transmittance measurements with respect to the angle of incidence is tested. This analysis allows not only for the separation of the variation from angular and spectral variables, but also for the identification of systematic errors in the measurements, which might be spectrally or angularly correlated.

The formalism of PCA is based on the diagonalization of the covariance matrix of a multidimensional correlated data set, $F = \{F_1, F_2, \ldots, F_N\}$, which allows the reduction of its dimensionality by representing the data in a new series of uncorrelated variables, or principal components. The elements of the covariance matrix are the covariances between the different variables involved, as defined in the literature [113]. This formalism assumes that any variable, or component, of the multidimensional data set can be expressed as a linear combination of the eigenvectors, e_{ij}, and the principal components, A_j, of the diagonalized covariance matrix as follows [114]:

$$F_i = \sum_{j=1}^{N} e_{ij} A_j, \quad (12)$$

where F_i represents a specific component of the multidimensional variable and the terms, A_j, represent an uncorrelated set of variables that contain all the information of the data.

In this work, the different variables F_i can be understood as the different measurements of the spectral reflectance or transmittance at different angles of incidence, where each wavelength, λ, represents a different realization of the variable. This approach is a variation of the one described in Ref. [115], which was developed to analyze spectral BRDF measurements. According to this approach, the measurement data of the spectral reflectance or transmittance of a specific glazing sample can be expressed as:

$$R(\lambda,\theta_i) = M(\theta_i) + \sum_{j=1}^{N} e_j(\theta_i) A_j(\lambda), \quad (13)$$

where $M(\theta_i)$ is the median of the values of the spectral reflectance or transmittance measurement, $R(\lambda,\theta_i)$, at a given angle of incidence, θ_i. The eigenvectors $e_j(\theta_i)$ contain the coefficients of the transformation from the base of the original correlated spectra to a new base of uncorrelated spectra, formed by the eigenspectra, or principal components, $A_j(\lambda)$, and they can be regarded as the weight of each component in the measurement data. The variance of the different eigenspectra is given by their corresponding eigenvalues.

5. Results and discussion

5.1. Measurements

As an example, the measurement results of a double-glazing IGU and a monolithic glass, identified as M2-02 and M1-02 (see Table 1), respectively, are shown in this section. Both are non-diffuse glazing samples, which means that the reflected or transmitted radiant flux propagates only in the corresponding regular direction. In this way, the obtained spectral reflectance and transmittance for $\theta_i = 5°$ and $\theta_i = 0°$, respectively, are represented in Fig. 7.

While the reflectance and the transmittance of the monolithic glass show a slight variation regarding the wavelength, the double-glazing IGU exhibits a significant difference between the visible and the infrared ranges. From the obtained values of the spectral reflectance and transmittance, the solar reflectance and transmittance can be estimated as follows:

$$R_{solar} = \frac{\int R(\lambda) E_{solar}(\lambda) d\lambda}{\int E_{solar}(\lambda) d\lambda}, \quad (14)$$

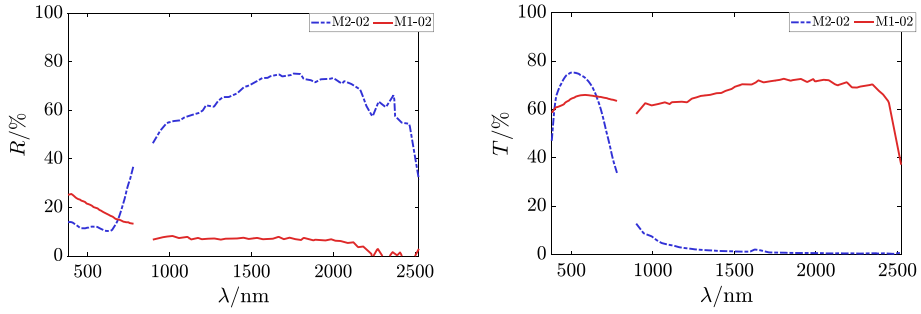

(a) Spectral reflectance. (b) Spectral transmittance.

Fig. 7. Spectral (a) reflectance and (b) transmittance of a double-glazing IGU (M2-02) and a monolithic glass (M1-02) for an angle of incidence of $\theta_i = 5°$ and $\theta_i = 0°$, respectively. The 780 nm - 900 nm gap in the measurement data is due to the operational limitation of the two spectroradiometers, as mentioned in Section 3.1.

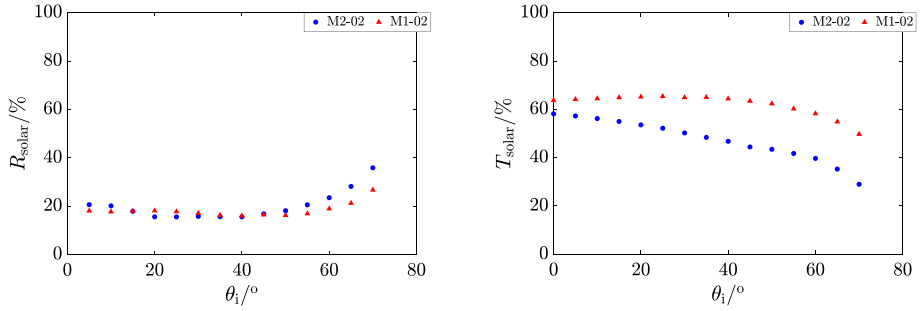

(a) Solar reflectance. (b) Solar transmittance.

Fig. 8. Solar (a) reflectance and (b) transmittance as a function of the angle of incidence of a double-glazing IGU (M2-02) and a monolithic glass (M1-02).

$$T_{\text{solar}} = \frac{\int T(\lambda) E_{\text{solar}}(\lambda) \mathrm{d}\lambda}{\int E_{\text{solar}}(\lambda) \mathrm{d}\lambda}, \tag{15}$$

where $E_{\text{solar}}(\lambda)$ is the spectral irradiance of the Sun on the surface of the Earth [116]. These quantities, thus, describe the portion of the incident solar energy that is reflected or transmitted by the glazing system. Fig. 8 shows the calculated solar reflectance and transmittance of the previous glazing samples from the spectral measurements for different angles of incidence. It must be noted that a linear interpolation of the missing data within the gap 780 nm - 900 nm had to be applied to estimate the integrated quantities, which introduces an uncertainty depending on the spectral distribution of the reflectance and transmittance of the samples. However, the evaluated samples are not expected to present abrupt variations in the refractive index within this gap. Thus, a negligible contribution to the uncertainty of the calculation is expected.

The results of Fig. 8 show that both samples present similar values of solar reflectance and transmittance, i.e., the portion of the incident solar energy that is being reflected or transmitted, contrary to the obtained results from the spectral measurements. However, this can be explained by the spectral distribution of solar irradiance, which has its maximum in the visible range, where the samples showed similar averaged values (see Fig. 7). In general, reflectance increases for higher angles of incidence while transmittance decreases. Nevertheless, the reflectance and transmittance variation with the angle of incidence is slightly higher in the double-glazing IGU than in the monolithic glass. This significantly affects the energy efficiency of buildings, since the sun irradiates the windows of the facade mainly at high angles, for which the difference between the performances of each sample is larger. In any case, the effect on the energy efficiency of buildings always depends on the latitude and the orientation of the specific building, which enhances the need for a detailed characterization of the angular dependence of the optical properties of glazing systems.

Regarding the results on the measurements of the diffuse glazing samples, two examples are shown in this section, both from the BRDF (Fig. 9) and the BTDF (Fig. 10) measurements. The selected samples for the plots correspond to a diffuse laminated glass (M3-07) and a diffuse double-glazing IGU (M3-11).

The results of the BRDF measurements show a different trend for each sample. The results for sample M3-07 indicate that the reflection of light is very diffuse at lower angles of incidence and increases at higher angles of incidence (see Fig. 9(a)), while the results for sample M3-11 show a different trend, the reflection of light at low angles of incidence is relatively more directional than at higher angles (see Fig. 9(b)). On the other hand, the results of the BTDF measurements are similar for both samples (see Fig. 10), and they show a constant directionality in the transmission of light with respect to the angle of incidence, contrary to the BRDF results. The number of selected geometries for the BTDF measurements might be coarse, as the maximum of the BTDF, which is around the regular direction, is not properly resolved. These measurements could be improved with a more detailed angular sampling, but it would require considerably more time and the aim of this work is to demonstrate the capabilities of the system and the relevance of these kinds of measurements, rather than provide a detailed BSDF characterization of the evaluated diffuse samples.

5.2. Model fitting

The results of the fitting of the analytical model, described in Section 4.1, to the measurement data of a subset of samples at 500 nm are shown in Fig. 11.

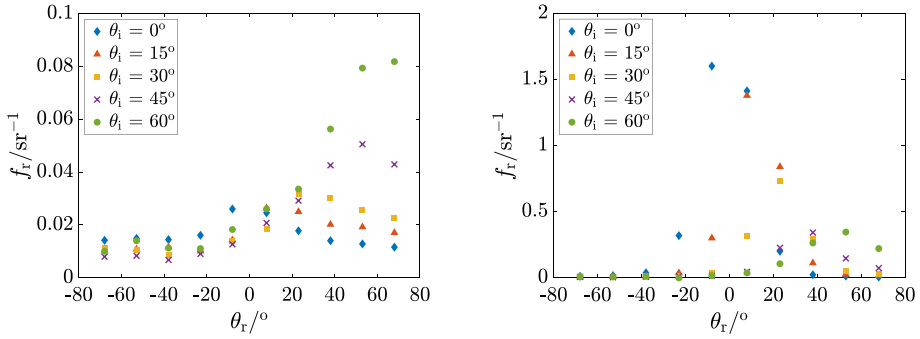

(a) M3-07. (b) M3-11.

Fig. 9. BRDF measurement values of sample (a) M3-07 and (b) M3-11, spectrally averaged, as a function of the collection angle for different angles of incidence.

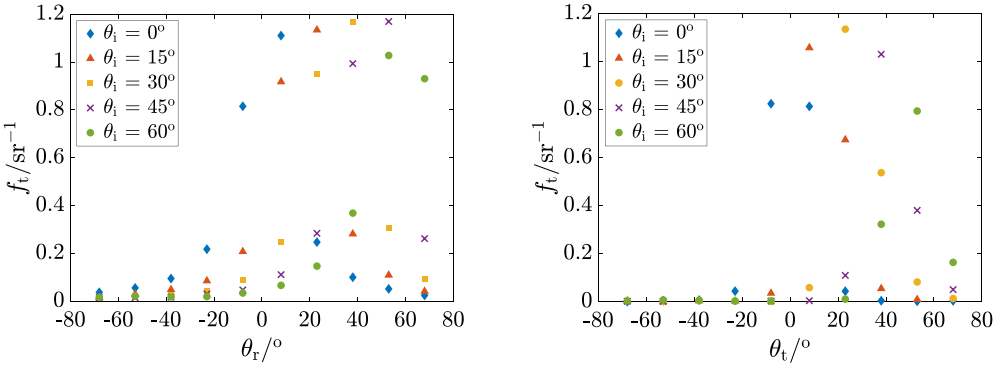

(a) M3-07. (b) M3-11.

Fig. 10. BTDF measurement values of sample (a) M3-07 and (b) M3-11, spectrally averaged, as a function of the collection angle for different angles of incidence.

The goodness of the fit is, in general, similar for all measurements, and it is quantified with the standard error of the estimate (SEE), defined as:

$$\mathrm{SEE} = \frac{1}{M_R M_T}\sqrt{\sum_{\theta_i \in M_R}\left[R\left(n,\overline{\sigma_a},\right)\theta_i - \hat{R}_{\theta_i}\right]^2 + \sum_{\theta_i \in M_T}\left[T\left(n,\overline{\sigma_a},\right)\theta_i - \hat{T}_{\theta_i}\right]^2}, \tag{16}$$

and the coefficient of determination, R^2, defined as:

$$R^2 = 1 - \frac{\sum_{\theta_i \in M_R}\left[\hat{R}_{\theta_i} - R\left(n,\overline{\sigma_a},\right)\theta_i\right]^2 + \sum_{\theta_i \in M_T}\left[\hat{T}_{\theta_i} - T\left(n,\overline{\sigma_a},\right)\theta_i\right]^2}{\sum_{\theta_i \in M_R}\left[\hat{R}_{\theta_i} - \overline{R}_{\theta_i}\right]^2 + \sum_{\theta_i \in M_T}\left[\hat{T}_{\theta_i} - \overline{T}_{\theta_i}\right]^2}, \tag{17}$$

where $\overline{R}_{\theta_i}$ and $\overline{T}_{\theta_i}$ represent the averages of the reflectance and transmittance measurements, respectively.

These indicators describe the quality of the fitting results. The first indicator, the SEE, represents the error of the estimates, i.e., the difference between the predicted values and the measured ones. This indicator must be compared with the values of the measured quantity, ranging between 0 and 1, in order to understand the relative deviation between the model and the measured data. The second indicator, the R^2, determines the portion of the variability of the measured quantity that is explained by the model. It usually ranges from 0 to 1, where 0 indicates a poor fit and 1 denotes a perfect fit, although negative values are also possible when the model cannot accurately explain a low variation of the measurement data.

The SEE and the R^2 of the fittings for all the evaluated non-diffuse samples are plotted in Fig. 12. In general, IGU samples show larger SEE and lower R^2, while monolithic samples present lower values of SEE, which depict lower errors in the estimates. This suggests that the observed deviations between the model and the measurements could be explained in part by systematic errors due to the methodological issues mentioned above, which are larger for thick samples (IGU) and large angles of incidence. One way to improve the efficacy of the model would be to use only the measurement values at low angles of incidence to fit the parameters, avoiding those angles at which systematic errors might considerably affect the measurement.

In particular, for the two triple-glazing IGU samples (M3-13 and M3-20, marked with * in Fig. 12), the model shows considerably higher deviations from the measurements (high SEE values). In addition, there are some specific cases in which SEE is very high, probably depicting an issue in the specific measurement (M1-16, M1-32, M3-06 and M3-19, marked with * in Fig. 12). On the other hand, there are some cases in which the coefficient of dependence R^2 presents negative values with a SEE not especially high (M1-01, M1-03, M1-05, M1-06 and M1-07, marked with ** in Fig. 12). In these cases, although the deviations of the predicted values from the measured ones might be low, the mean of the measured data provides a better estimation of the outcome than the model, since the variation of reflectance and transmittance regarding the angle of incidence in these samples is very low (see Fig. 11(a)).

The measurement data do not allow a relationship between a higher SEE and the type of coating to be found. In general, systematic deviations between the measurement data and the fitted model are not observed. We must note here that the SEE values are not large. They are below 0.02 for almost all samples, and there is only one sample for which the

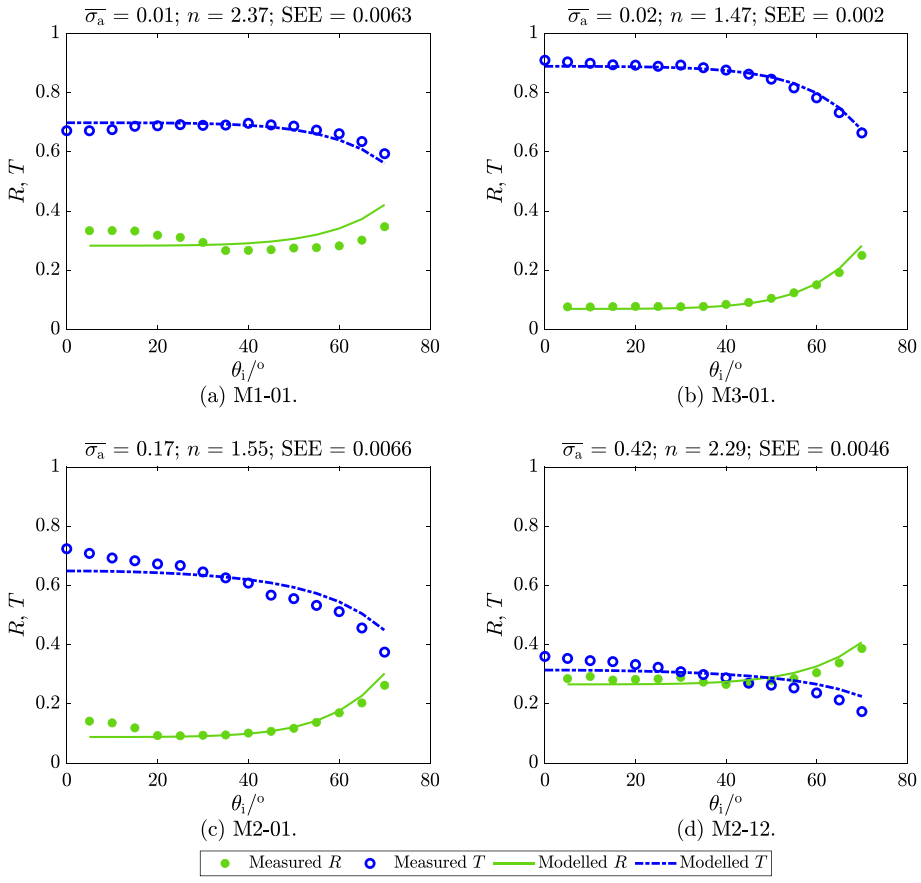

Fig. 11. Model fittings of samples (a) M1-01, (b) M3-01, (c) M2-01 and (d) M2-12 for an irradiation wavelength of 500 nm. The obtained fitting parameters (n and $\overline{\sigma_a}$) and the standard error of the estimate (SEE) for each sample are specified at the top of each plot.

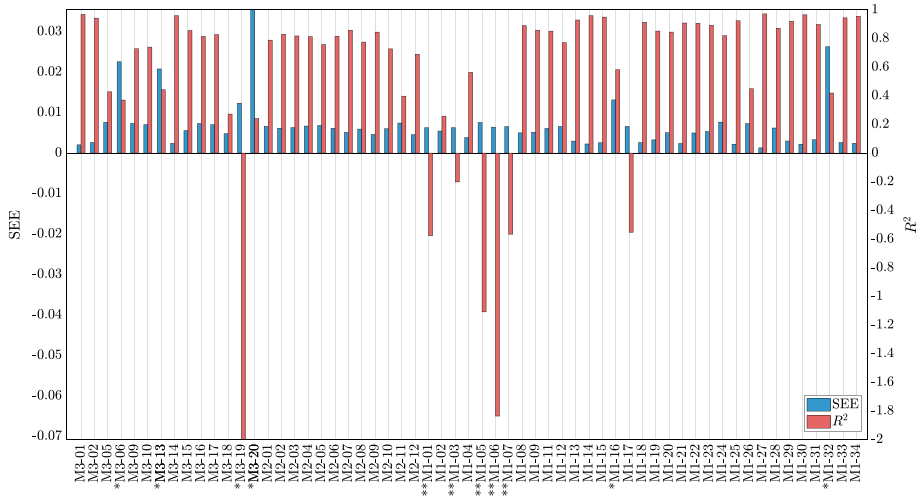

Fig. 12. SEE and R^2 of the fitting for an irradiation wavelength of 500 nm and all the evaluated non-diffuse samples. Those sample marked with * exhibit relatively poor values for both indicators of the goodness of the fitting, while those marked with ** exhibit poor values for the indicator R^2 but normal values for the SEE.

SEE is over 0.03. Taking into account that reflectance and transmittance values range from 0 to 1, this indicator depicts a good fit in all cases.

5.3. Discussion on PCA

As an example of the application of the PCA formalism described in Section 4.2, results for the monolithic sample M1-02 are shown in Fig. 13, which should be interpreted in combination with Eq. (13).

The PCA of the reflectance measurements of sample M1-02 shows that more than 92% of the variance of the measurement data can be described with only one eigenspectra, PC 1, which describes the spectral component of the measurements equally for all the angles of incidence, as depicted by the values of its corresponding eigenvector. In the case of the transmittance measurements, more than 84% of the total variance is described by the eigenspectra PC 1, whose corresponding eigenvector

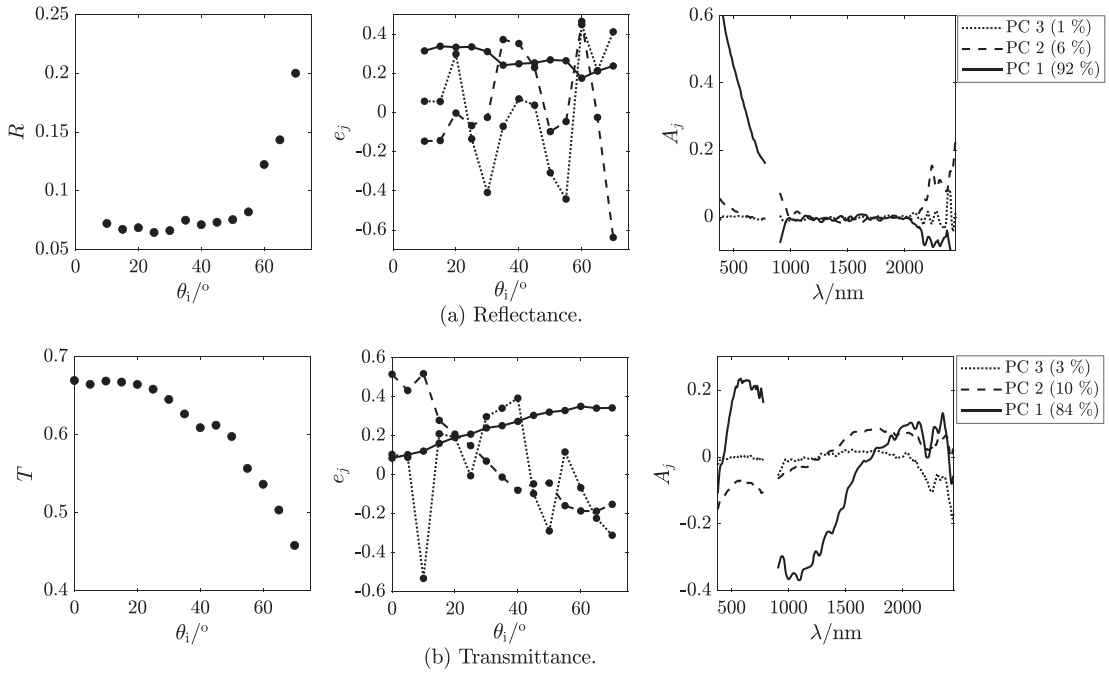

Fig. 13. Principal components analysis of the (a) reflectance and (b) transmittance measurements of the monolithic sample M1-02. In each case, the plot on the left shows the median of the spectral reflectance or transmittance for each angle of incidence, the plot on the middle shows the values of the eigenvectors of the three main principal components (PC), which correspond to the PCs whose variances are the highest, at each angle of incidence, and the plot on the right shows those three main PC, or eigenspectra. The legend indicates the percentage of the total variance that each PC represents.

shows a proportional increase regarding the angle of incidence. This component seems to describe the general relative spectral distribution of the measured quantity, which is modulated for the different angles of incidence. This is consistent in all the samples, although the spectral distribution and its modulation through the different angles of incidence are specific to each sample.

The rest of the principal components might depict some specific artifacts in the spectral information of the measurements which depend strongly on the specific sample and measurement. The analysis of the physical meaning of these components is complex and has not been addressed in this work.

Overall, Fig. 13 shows that more than 95% of the total variance of the data can be described with only three principal components in both cases. This indicates that the spectral reflectance or transmittance measurements of sample M1-02, across all angles of incidence, can be represented by three eigenspectra and their corresponding eigenvectors. Our results show that this conclusion can be generalized to the other samples. This enables a reduction of the input dimensionality in simulation tools and might be used to improve database interoperability.

6. Conclusions

A methodology for evaluating the dependence of the spectral reflectance and transmittance of glazing samples on the angle of incidence has been proposed, and measurements of spectral reflectance and transmittance of more than 60 commercial glazing samples, which are representative of those used in new and existing constructions, have been carried out. The results of these measurements show a significant dependence of the reflectance and transmittance of those glazing samples on the angle of incidence. Thus, including their reflectance and transmittance values at different angles of incidence in energy simulation software would benefit the energy efficiency assessment. However, the inclusion of these data in commercial simulation software is not direct, and requires further studies on the implementation of integration methods. In addition, the results of the measurements of diffuse glazing samples provide additional information on the reflected and transmitted radiant flux distributions, which can be very useful for lighting optimization.

The presented measurements in this work exhibit a gap between 780 nm and 900 nm due to the operational limitations of the spectroradiometers. However, since the evaluated samples do not present abrupt variations in the refractive index within this gap, the missing data could be obtained from a parametrization of the spectral dependence of the parameters of the presented model, which is an ongoing research. In addition, some methodological issues in the measurement have been identified, and solutions have been proposed. However, the measurement of IGU samples is still challenging and should be limited to a maximum angle of incidence, depending on the number of layers and the thickness of the sample, which might be sufficient for the proper application of the model. According to the conventional IGU samples measured in this work, an angle of incidence higher than 45° should not be exceeded to avoid the main methodological issues. This, however, depends on the thickness of the sample, the angle of incidence and the irradiation spot size. Thus, one could calculate the maximum angle of incidence for their measurements, at which the second beam generated by the inter-reflections falls outside of the FOV of the detection system, through simple trigonometry.

A method for applying a principal components analysis to the measurement data has been proposed and the results on one of the samples show that the relevant information about the spectral reflectance and transmittance and their dependence on the angle of incidence could be described even with only three principal components, which reduces the amount of data by up to four times and benefits the data exchange. It has also been demonstrated that such analysis allows for separating the variation from angular and spectral variables, benefiting a better understanding of the data. However, a thorough analysis of the physical meaning of the principal components of the different kinds of glazing is not addressed in this work, and it could be addressed in future research.

Finally, a simple physics-based model has been used for non-diffuse glazing samples, which can be fitted to the measurements with only two

parameters for each wavelength or each spectral integration, as in the case of solar reflectance and transmittance. These two parameters convey information about reflectance, transmittance and their dependence on the angle of incidence in a very simple way. Although the model is not able to describe the physical properties of the evaluated glazing materials, its main advantage lies in the low number of parameters that allow the number of measurements needed to evaluate the reflectance and transmittance of glazing samples to be reduced, avoiding those geometries presenting methodological issues. The results shown in Section 5.2 indicate that the model is capable of reproducing the optical properties of non-diffuse glazing systems, as the few observed discrepancies are mainly attributable to measurement errors. In the case of IGU samples, a more suitable approach would be to fit the model only using the measured values obtained at angles of incidence below 45°, assuming that these values are not significantly affected by the methodological issues. However, the applicability of the model is limited to single wavelengths or integrated spectral ranges, which precludes the analysis of spectral interference effects. Besides, this research does not take into account the operability of glazing samples under different climatic conditions, which can affect the effective refractive index and absorption coefficient of glazing systems. In this way, the proposed model could be improved by adding a thin layer of water on the outside surface to control the humidity of the air.

Overall, this research establishes a benchmark for angular evaluation of spectral reflectance and transmittance of glazing systems and outlines the path forward for future research. Future efforts include the extension of the methodology to different climates and different types of glazing materials or the search of the optimal geometrical configurations for the measurements to fit the model. Such efforts should also address improving format compatibility and retrieval efficiency of the data within mainstream building-simulation platforms, thereby maximizing the practical impact of this research.

CRediT authorship contribution statement

Pablo Santafé-Gabarda: Writing – review & editing, Writing – original draft, Visualization, Validation, Software, Methodology, Investigation, Formal analysis, Data curation. **Jorge Álvarez:** Writing – review & editing, Writing – original draft, Resources, Investigation. **Adolfo Muñoz:** Writing – review & editing, Writing – original draft, Methodology, Formal analysis, Conceptualization. **M. Mar Barbero-Barrera:** Writing – review & editing, Project administration, Funding acquisition, Conceptualization. **Joaquín Campos:** Writing – review & editing, Funding acquisition. **Alejandro Ferrero:** Writing – review & editing, Writing – original draft, Validation, Supervision, Software, Resources, Project administration, Methodology, Funding acquisition, Formal analysis, Data curation, Conceptualization.

Declaration of competing interest

The authors declare that they have no known competing financial interests or personal relationships that could have appeared to influence the work reported in this paper.

Acknowledgments

This work is part of the project TED2021-129661B-C21, funded by the Spanish Ministry of Science, Innovation and Universities, grant number MCIN/AEI/10.13039/501100011033, and the European Union “NextGenerationEU”/PRTR economic recovery package. In addition, we would like to acknowledge Pedro Mazón (Saint-Gobain) and Igino Rocchio and Arturo Benini (Pilkington) for their support in providing some of the samples used in this study. Some of the authors would also like to acknowledge the project JRP 23IND14 xDDiff, which has received funding from the European Partnership on Metrology, co-financed by the European Union’s Horizon Europe Research and Innovation Programme and by the Participating States.

Data availability

Data underlying the results presented in this paper are available in Ref. [102].

References

[1] European Commission, Buildings. energy, Apr 2018. https://energy.ec.europa.eu/topics/energy-efficiency.
[2] European Union, Directive (EU) 2024/1275 of the european parliament and of the council of 24 April 2024 on the energy performance of buildings, official jorunal of the european union l series, 2024/1275, 2024. https://eur-lex.europa.eu/eli/dir/2024/1275/oj.
[3] EU Building Stock Observatory, Factsheets, 2024. https://building-stock-observatory.energy.ec.europa.eu/factsheets/.
[4] Energy consumption in households - statistics explained - eurostat, https://ec.europa.eu/eurostat/statistics-explained/index.php?title=Energy_consumption_in_households.
[5] International Energy Agency, Energy efficiency, 2023. https://iea.blob.core.windows.net/assets/dfd9134f-12eb-4045-9789-9d6ab8d9fbf4/EnergyEfficiency2023.pdf.
[6] W.Y. Hong, B.N. Ni, M. Nura, L. Rahmat, B. Darussalam, Energy consumption, CO_2 emissions and electricity costs of lighting for commercial buildings in southeast Asia, Scientific Rep. 12 (2022) 13805.
[7] International Energy Agency, Global electricity consumption in lighting in the net zero scenario, 2010–2030, 2023. https://www.iea.org/data-and-statistics/charts/global-electricity-consumption-in-lighting-in-the-net-zero-scenario-2010-2030.
[8] A. Gevorgian, S. Pezzutto, S. Zambotti, S. Croce, U.F. Oberegger, R. Lollini, A. Müller, European Building Stock Analysis, Tech. rep., Eurac Research, 2021.
[9] M. González-Torres, L. Pérez-Lombard, J.F. Coronel, I.R. Maestre, D. Yan, A review on buildings energy information: trends, end-uses, fuels and drivers, Energy Rep. 8 (2022) 626–637.
[10] B. Arranz, Energy Performance Optimization of Window Systems. Proposal of an Indicator as a Tool for an Integrated Analysis of Glazing, (Ph.D. thesis), Universidad Politécnica de Madrid, 2013.
[11] R. Caro, L. Cruz, P.S. Naharro, S. Muelas, A. Martínez, K.K. Sancho, E. Cuerda, M. Del Mar Barbero-Barrera, A. LaTorre, Prescriptive tool for Zero-Emissions building fenestration design using hybrid metaheuristic algorithms, unpublished. Pre-print available at SSRN, 2024. https://papers.ssrn.com/abstract=4965549.
[12] D. Arasteh, S. Selkowitz, J. Apte, M. LaFrance, Zero energy windows, in: Proceedings of the 2006 ACEEE Summer Study on Energy Efficiency in Buildings, 2006.
[13] J. Mustafa, S. Alqaed, M. Sharifpur, J. Meyer, Optimization of window solar gain for a building with less cooling load, Case Stud. Therm. Eng. 53 (2024) 103890.
[14] Y. Mo, C. Wang, M.A. Kassem, D. Wang, Z. Chen, Optimizing window configurations for Energy-Efficient buildings with aluminum alloy frames and Helium-Filled insulating glazing, Sustainability 16 (2024) 6522.
[15] H. Yuk, J.Y. Choi, S. Yang, S. Kim, Balancing preservation and utilization: window retrofit strategy for energy efficiency in historic modern building, Build. Environ. 259 (2024) 111648.
[16] M. de Luxán García de Diego, M.B. Barrera, G.G. Muñoz, E.R. López, Estudio para LA elaboración del plan RENOVE de acristalamientos EN viviendas de LA comunidad de Madrid, in: SB10mad: Edificación Sostenible. Revitalización Y Rehabilitación De Barrios, 2010.
[17] F. Kheiri, Optimization of building fenestration and shading for climate-based daylight performance using the coupled genetic algorithm and simulated annealing optimization methods, Indoor Built Environ. 30 (2019) 195–214.
[18] W. El-Menshawi, A.F. Bakr, A.A. Fathi, Optimizing fenestration systems in residential buildings: a parametric analysis of Egyptian energy codes’ impact on thermal comfort, J. Eng. Res. 8 (2024) 36.
[19] Instituto para la Diversificación y Ahorro de Energía: Madrid, Guía práctica de LA energía. Consumo eficiente y responsable, 2014.
[20] J. Pereira, M.G. Gomes, A.M. Rodrigues, M. Almeida, Thermal, luminous and energy performance of solar control films in single-glazed windows: use of energy performance criteria to support decision making, Energy Build. 198 (2019) 431–443.
[21] Z. Yang, B. Liu, H. Zhao, Energy saving in building construction in China: a review, Int. J. Green Energy 1 (2004) 209–225.
[22] S. Forughian, M.T.S. Aiini, Comparative study of single-glazed and double-glazed windows in terms of energy efficiency and economic expenses, J. Hist. Cult. Art Res. 6 (2017) 879.
[23] Y. Abdou, Y.O.U.N.G.K.I. KIM, A. Abdou, R. Anabtawi, Energy optimization for fenestration design: Evidence-Based retrofitting solution for office buildings in the UAE, Buildings 12 (2022) 1541.
[24] Y.J. Lee, S.H. Kim, J.H. Ryu, K.H. Lee, Optimizing window glass design for energy efficiency in South Korean office buildings: a hierarchical analysis using energy simulation, Buildings 13 (2023) 2850.
[25] European Union, Directive (EU) 2023/1791 of the european parliament and of the council of 13 September 2023 on energy efficiency and amending regulation (EU) 2023/955 (recast) (text with EEA relevance), official jorunal of the european union l series, 231/1, 2023. http://data.europa.eu/eli/dir/2023/1791/oj.
[26] G. Feng, D. Chi, X. Xu, B. Dou, Y. Sun, Y. Fu, Study on the influence of window-wall ratio on the energy consumption of nearly zero energy buildings, Procedia Eng. 205 (2017) 730–737.
[27] Y. Fang, S. Cho, Design optimization of building geometry and fenestration for daylighting and energy performance, Solar Energy 191 (2019) 7–18.

[28] A.R. Hassani, P. Domenighini, E. Belloni, T. Ihara, C. Buratti, Evaluation of the solar heat gain coefficient of innovative aerogel glazing systems: experimental campaigns and numerical results, J. Build. Eng. 62 (2022) 105354.

[29] A. Ahmad, O. Prakash, L.S. Brar, K. Irshad, S.M.M. Hasnain, P. Paramasivam, A.G. Ayanie, Effect of wall, roof, and Window-to-Wall ratio on the cooling and heating load of a building in India, Energy Sci. Eng. 13 (2025) 1255–1279.

[30] J. Shaeri, A. Habibi, M. Yaghoubi, A. Chokhachian, The optimum Window-to-Wall ratio in office buildings for hot;humid, hot;dry, and cold climates in Iran, Environments 6 (2019) 45.

[31] S. Sayadi, A. Hayati, M. Salmanzadeh, Optimization of Window-to-Wall ratio for buildings located in different climates: an IDA-indoor climate and energy simulation study, Energies 14 (2021) 1974.

[32] X. Yu, Y. Su, Daylight availability assessment and its potential energy saving estimation –a literature review, Renew. Sustain. Energy Rev. 52 (2015) 494–503.

[33] S.A. Moghaddam, C. Serra, M.G. da Silva, N. Simões, Comprehensive review and analysis of glazing systems towards nearly Zero-Energy buildings: energy performance, thermal comfort, Cost-Effectiveness, and environmental impact perspectives, Energies 16 (2023) 6283.

[34] S. Amirkhani, A. Bahadori-Jahromi, A. Mylona, P. Godfrey, D. Cook, Impact of Low-E window films on energy consumption and CO_2 emissions of an existing UK hotel building, Sustainability 11 (2019) 4265.

[35] S.A. Moghaddam, M. Mattsson, A. Ameen, J. Akander, M.G. Da Silva, N. Simões, Low-Emissivity window films as an energy retrofit option for a historical stone building in cold climate, Energies 14 (2021) 7584.

[36] R. Bruno, Optimization of glazing systems in Non-Residential buildings: the role of the optical properties of air-conditioned environments, Build. Environ. 126 (2017) 147–160.

[37] X. Kong, W. Yao, J. Duan, L. Jiang, Y. Dong, D. Lin, W. Gao, Development of a solar radiation model for quantifying spectral transmittance and loss rates of nanofluid-based glass devices, Renew. Energy 252 (2025) 123512.

[38] M. Krarti, Design optimization of smart glazing optical properties for office spaces, Appl. Energy 308 (2022) 118411.

[39] S. Lu, A. Tzempelikos, Realistic glazing/window properties for minimizing building energy use through simulation-based optimization, Appl. Energy 393 (2025) 125974.

[40] Y. Zhai, Y. Wang, Y. Huang, X. Meng, A multi-objective optimization methodology for window design considering energy consumption, thermal environment and visual performance, Renewable Energy 134 (2019) 1190–1199.

[41] EN 17037:2018 + a1. Daylight in buildings

[42] H.F.O. Müeller, Daylighting, Elsevier Inc., 2013, pp. 227–255.

[43] M. Fakhari, R. Fayaz, S. Asadi, Lighting preferences in office spaces concerning the indoor thermal environment, Front. Archit. Res. 10 (2021) 639–651.

[44] O.K. Overen, E.L. Meyer, G. Makaka, Indoor daylighting and thermal response of a passive solar building to selective components of solar radiation, Buildings 11 (2021) 34.

[45] A. Ahmad, O. Prakash, A. Kumar, S.M.M. Hasnain, P. Verma, A. Zare, G. Dwivedi, A. Pandey, Dynamic analysis of daylight factor, thermal comfort and energy performance under clear sky conditions for building: an experimental validation, Mater. Sci. Energy Technol. 5 (2022) 52–65.

[46] M. Boubekri, Daylighting, Architecture and Health, Routledge, 2008.

[47] Ö.K. Madan, K. Chamilothori, J. van Duijnhoven, M.P.J. Aarts, Y.A. de Kort, Restorative effects of daylight in indoor environments – a systematic literature review, J. Environ. Psychol. 97 (2024) 102323.

[48] Z. Javani, R. Madani, I. Hojat, R. Zadeh, The relationship between daylight and happiness for women in residential districts of isfahan, Iran, Environ. Qual. Manag. 28 (2019) 103–110.

[49] A. Hedge, D. Nou, Worker reactions to electrochromic and low e glass office windows, Ergon. Int. J. 2 (2018).

[50] R.P. Leslie, Capturing the daylight dividend in buildings: why and how? Build. Environ. 38 (2003) 381–385.

[51] K.A. Mazurek, L. Li, R.J. Klein, S. Rong, A.F. Mullan, D.T. Jones, E.K.S. Louis, G.A. Worrell, C.Y. Chen, Investigating the effects of indoor lighting on measures of brain health in older adults: protocol for a cross-over randomized controlled trial, BMC Geriatrics 24 (2024) 816.

[52] P. Varma, S.A. Rahman, Lighting the path forward: the value of sleep- and circadian-informed lighting interventions in shift work, Sleep 47 (2024) 1–4.

[53] A. Li, X. Wei, Y. Xie, Y. Ren, X. Zhu, M. Liu, S. Liu, Light exposure and its applications in human health, J. Biophoton. 17 (2024) e202400023.

[54] Eurostat, Energy consumption in households, 2024. https://ec.europa.eu/eurostat/statistics-explained.

[55] International Energy Agency, CO_2 emissions and emissions intensity for lighting in the net zero scenario, 2000-2030, 2023. https://www.iea.org/data-and-statistics/charts.

[56] A. De Almeida, B. Santos, P. Bertoldi, M. Quicheron, Solid state lighting review – potential and challenges in Europe, Renew. Sustain. Energy Rev. 34 (2014) 30–48.

[57] S.T. Tzeiranaki, P. Bertoldi, M. Economidou, E.L. Clementi, M. Gonzalez-Torres, Determinants of energy consumption in the tertiary sector: evidence at european level, Energy Rep. 9 (2023) 5125–5143.

[58] D.G. Zenginis, K.J. Kontoleon, Influence of orientation, glazing proportion and zone aspect ratio on the thermal performance of buildings during the winter period, Environ. Sci. Pollut. Res. 25 (2018) 26736–26746.

[59] Y. Pan, M. Zhu, Y. Lv, Y. Yang, Y. Liang, R. Yin, Y. Yang, X. Jia, X. Wang, F. Zeng, S. Huang, D. Hou, L. Xu, R. Yin, X. Yuan, Building energy simulation and its application for building performance optimization: a review of methods, tools, and case studies, Adv. Appl. Energy 10 (2023) 100135.

[60] Z. Liu, H. Luo, Y. Zhang, T. Luo, X. Yang, A review of simulation software for energy systems: design, functionality, and applications, Therm. Sci. Eng. Prog. 53 (2024) 102760.

[61] C. Eon, J.K. Breadsell, J. Byrne, G.M. Morrison, The discrepancy between as-built and as-designed in energy efficient buildings: a rapid review, Sustainability 12 (2020) 6372.

[62] A.C. Menezes, A. Cripps, D. Bouchlaghem, R. Buswell, Predicted VS. Actual energy performance of non-domestic buildings: using post-occupancy evaluation data to reduce the performance gap, Appl. Energy 97 (2012) 355–364.

[63] Z. Zheng, J. Zhou, Z. Jiaqin, Y. Yang, F. Xu, H. Liu, Review of the building energy performance gap from simulation and building lifecycle perspectives: magnitude, causes and solutions, Dev. Built Environ. 17 (2024) 100345.

[64] P.K. Chaturvedi, N. Kumar, R. Lamba, Finding the gaps in design strategies and technological advancements for net-zero energy buildings development in India, Energy Environ. 35 (2024) 3880–3920.

[65] N. Aste, H.E. Huerto-Cardenas, C. Del Pero, F. Leonforte, M. Buzzetti, R.S. Adhikari, E. Montevecchio, C.L.S. Blavier, Energy efficiency in buildings: the gap between energy certification methods and real performances, Energies 18 (2025) 6015.

[66] M.M. Barbero-Barrera, A.J.C. Santos, M.R. Veiga, The appearance and luminous properties of lime and gypsum pastes: a comparative analysis of different methods of measurement, Constr. Build. Mater. 221 (2019) 562–572.

[67] V. Costanzo, F. Nocera, G. Evola, C. Buratti, A.L. Faro, L. Marletta, P. Domenighini, Optical characterization of historical coloured stained glasses in winter gardens and their modelling in daylight availability simulations, Sol. Energy. 243 (2022) 22–34.

[68] H.M. Sacht, L. Bragança, M. Almeida, R. Caram, Specification of glazings for façades based on spectrophotometric characterization of transmittance, Sustainability (Switz.) 13 (May 2021).

[69] J.C.P. dos Santos, M. Roriz, Influência do ângulo de incidência na transmitância de luz natural através de materiais transparentes, Amb. Constr. 7 (2007) 123–135.

[70] J.P. dos Santos, M. Roriz, Influência do ângulo de incidência nos ganhos de calor solar através de materiais transparentes, Ambiente Construíddo 12 (2012) 149–161.

[71] S.S. Ghosh, P.K. Biswas, S. Neogi, Effect of solar radiation at various incident angles on transparent conducting antimony doped indium oxide (IAO) film developed by sol–gel method on glass substrate as heat absorbing window glass fenestration, Solar Energy 109 (2014) 54–60.

[72] Windows & Daylighting, Berkeley Lab, International glazing database, https://windows.lbl.gov/igdb-downloads.

[73] National Fenestration Rating Council, USA, Test method for determining the solar optical properties of glazing materials and systems, 2013.

[74] CIE S 017/E:2020, ILV: international lighting vocabulary, 2020, second.

[75] D.B. Judd, Terms, definitions and symbols in reflectometry, J. Opt. Soc. Am. 57 (1967).

[76] F.E. Nicodemus, J.C. Richmond, J.J. Hsia, I.W. Ginsberg, T. Limperis, Geometrical considerations and nomenclature for reflectance, NBS Monograph 160, U.S. Department of Commerce, National Bureau of Standards (Oct, 1977).

[77] G. Obein, R. Bousquet, M.E. Nadal, New NIST reference goniospectrometer, in: Proc. SPIE 5880, Optical Diagnostics, SPIE, 2005, p. 58800T.

[78] A.M. Rabal, A. Ferrero, J. Campos, J.L. Fontecha, A. Pons, A.M. Rubīo, A. Corróns, Automatic gonio-spectrophotometer for the absolute measurement of the spectral BRDF at in- and out-of-plane and retroreflection geometries, Metrologia 49 (2012) 213–223.

[79] D. Hünerhoff, U. Grusemann, A. Höpe, New robot-based gonioreflectometer for measuring spectral diffuse reflection, Metrologia 43 (2006) S11.

[80] F.B. Leloup, S. Forment, P. Dutré, M.R. Pointer, P. Hanselaer, Design of an instrument for measuring the spectral bidirectional scatter distribution function, Appl. Opt. 47 (2008) 5454–5467.

[81] R. Baribeau, W.S. Neil, É. Côté, Development of a robot-based gonioreflectometer for spectral brdf measurement, J. Mod. Opt. 56 (13) (2009) 1497–1503.

[82] N. Matsapey, J. Faucheu, M. Flury, D. Delafosse, Design of a gonio-spectrophotometer for optical characterization of gonio-apparent materials, Meas. Sci. Technol. 24 (2013) 065901.

[83] M. Arıcı, M. Tükel, Ç. Yıldız, D. Li, H. Karabay, Is the thermal transmittance of air-filled inclined multi-glazing windows similar to that of vertical ones? Energy and Buildings 229 (2020) 110515.

[84] https://www.iso.org/standard/89258.html.

[85] J. de Boer, E.S. Lee, N. Gentile, W. Osterhaus, Integrated solutions for daylighting and electric lighting, Energy and Buildings 277 (2022) 112575.

[86] P. Apian-Bennewitz, J. de Boer, B. Bueno, B. Deroisy, Y. Fang, D. Geisler-Moroder, L.O. Grobe, J.C. Jonsson, E.S. Lee, Z. Tian, T. Wang, G.J. Ward, H.R. Wilson, Y. Wu, Analysis and Evaluation of BSDF Characterization of Daylighting Systems, Tech. rep., International Energy Agency, 2021, https://doi.org/10.18777/ieashc-task61-2021-0012

[87] M. Rubin, R. Powles, K. Von Rottkay, Models for the angle-dependent optical properties of coated glazing materials, Solar Energy 66 (1999) 267–276.

[88] A. Roos, J. Karlsson, P.A. van Nijnatten, M.G. Hutchins, P. Polato, E. Nichelatti, M. Montecchi, F. Olive, C. Anderson, Angular dependent optical properties of coated glazings — validation of two predictive algorithms, Sol. Switch. Mater. 4458 (2001) 19–28.

[89] M.G. Hutchins, A.J. Topping, C. Anderson, F. Olive, P. Van Nijnatten, P. Polato, A. Roos, M. Rubin, Measurement and prediction of angle-dependent optical properties of coated glass products: results of an inter-laboratory comparison of spectral transmittance and reflectance, Thin Solid Films 392 (2001) 269–275.

[90] I.R. Maestre, J.L. Molina, A. Roos, J.F. Coronel, A single-thin-film model for the angle dependent optical properties of coated glazings, Solar Energy 81 (2007) 969–976.
[91] J.T. Kider, B. Walter, S. Fang, E. Sekkin, D.P. Greenberg, Transition portal for daylighting calculations in early phase design, Energy and Buildings 198 (2019) 353–363.
[92] A.A.W. Hawila, A. Merabtine, N. Troussier, R. Bennacer, Combined use of dynamic building simulation and metamodeling to optimize glass facades for thermal comfort, Build. Environ. 157 (2019) 47–63.
[93] E.O. do Nascimento, M.J.P. Becatti, L.V.E. Caldas, L.N. de Oliveira, Design of experiments (DoE) method for solar protective films via UV–vis and NIR spectrophotometry measurements, J. Lumin. 242 (2022) 118558.
[94] L. Zur, C. Armellini, S. Belmokhtar, A. Bouajaj, E. Cattaruzza, A. Chiappini, F. Coccetti, M. Ferrari, F. Gonella, G.C. Righini, E. Trave, A. Vomiero, F. Enrichi, Comparison between glass and glass-ceramic silica-hafnia matrices on the down-conversion efficiency of tb3+/yb3+ rare earth ions, Opt. Mater. 87 (2019) 102–106.
[95] V.R. Maduru, S. Shaik, Laminated glazing for buildings: energy saving, natural daylighting, and CO_2 emission mitigation prospective, Environ. Sci. Pollut. Res. 29 (2022) 14299–14315.
[96] R.S. Zakirullin, Chromogenic materials in smart windows for angular-selective filtering of solar radiation, Mater. Today Energy 17 (2020) 100476.
[97] G.K. Dalapati, S. Masudy-Panah, S.T. Chua, M. Sharma, T.I. Wong, H.R. Tan, D. Chi, Color tunable low cost transparent heat reflector using copper and titanium oxide for energy saving application, Scientific Rep. 6 (2016) 1–14.
[98] A.M. Almogbel, S. Hussain, A. Kalendar, Evaluation of the effect of nanocoated window glazing films on the thermal behavior of buildings, Heat Transfer 50 (3) (2021) 2667–2685.
[99] H. Zong, H. Liu, L. Yan, Y. Yin, L. Bian, C. Kang, G. Cao, M. Li, Synchronized improvements of luminous transmittance and solar modulation ability of vo2 films by employing sno2 buffer layers, Thin Solid Films 709 (2020) 138174.
[100] P. Ashok, Y.S. Chauhan, A. Verma, High infrared reflectance modulation in vo2 films synthesized on glass and ITO coated glass substrates using atmospheric oxidation of vanadium, Opt. Mater. 110 (2020) 110438.
[101] M. Rubin, K. Von Rottkay, R. Powles, Window Optics, Solar Energy 62 (1998) 149–161.
[102] J.O. Álvarez Pérez, P. Santafé, A. Ferrero, Database of glazing systems for building [dataset], 2025. https://digital.csic.es/handle/10261/384294.
[103] L.A.B. Pilkington, Review lecture: the float glass process, in: Proceedings of the Royal Society of London. A. Mathematical and Physical Sciences, vol. 314, The Royal Society London, 1969, pp. 1516.
[104] Hamamatsu. Super-quiet Xenon lamp, Super-quiet Mercury-Xenon lamp [specifications sheet]. Hamamatsu photonics, https://www.hamamatsu.com/content/dam/hamamatsu-photonics/sites/documents/99_SALES_LIBRARY/etd/Xe-HgXe_TLS1016E.pdf.
[105] https://www.oceanoptics.com/spectrometer/nirquest2-5/.
[106] J.M. Palmer, B.G. Grant, Propagation of Optical Radiation, SPIE, 2009, pp. 11–61.
[107] J. Krochmann, P. Polato, F. Geotti-Bianchini, D. Gundlach, J.J. Hsia, L. Morren, H. Terstiege, J. Verrill, Practical Methods for the Measurement of Reflectance and Transmittance, Tech. rep., International Commission on Illumination, CIE 130-1998, 1998.
[108] N. Basic, E. Molloy, A. Koo, A. Ferrero, P.S. Gabarda, L. Gevaux, G. Porrovecchio, A. Schirmacher, M. Šmíd, P. Blattner, K.-O. Hauer, T. Quast, J. Campos, G. Obein, Intercomparison of bidirectional reflectance distribution function measurements at in- and out-of-plane geometries, Appl. Opt. 62 (2023) 3320–3329.
[109] J. Fu, A. Ferrero, T. Quast, M. Esslinger, P. Santafé-Gabarda, N. Tejedor, J. Campos, L. Gevaux, G. Obein, R. Aschan, F. Manoocheri, E. Ikonen, G. Porrovecchio, M. Šmíd, E. Molloy, A. Koo, S.A. Jensen, R. Oser, J. Audenaert, Y. Meuret, S. Källberg, I. Gozhyk, T. Kraus, A. Schirmacher, Survey of bidirectional transmittance distribution function measurement facilities by multilateral scale comparisons, Metrologia 61 (2024) 035006.
[110] O.S. Heavens, Principles of optics. By born and wolf. 1964.(pergamon), Math. Gaz. 49 (370) (1965) 485.
[111] W. Jakob, S. Speierer, N. Roussel, M. Nimier-David, D. Vicini, T. Zeltner, B. Nicolet, M. Crespo, V. Leroy, Z. Zhang, Mitsuba 3 renderer, 2022. https://mitsuba-renderer.org.
[112] D.P. Kingma, J. Ba, Adam: A method for stochastic optimization, arXiv preprint arXiv:1412.6980, 2014.
[113] Joint Committee for Guides in Metrology (JCGM), Evaluation of measurement data – supplement 2 to the “guide to the expression of uncertainty in measurement” – extension to any number of output quantities, JCGM 102:2011, 2011.
[114] J.M. López-Alonso, J. Alda, E. Bernabéu, Principal-component characterization of noise for infrared images, Appl. Opt. 41 (2002) 320–331.
[115] A. Ferrero, J. Campos, A.M. Rabal, A. Pons, M.L. Hernanz, A. Corróns, Principal components analysis on the spectral bidirectional reflectance distribution function of ceramic colour standards, Opt. Express. 19 (2011) 19199–19211.
[116] G. Thuillier, L. Floyd, T.N. Woods, R. Cebula, E. Hilsenrath, M. Hersé, D. Labs, Solar irradiance reference spectra, in: J.M. Pap, P. Fox, C. Frohlich, H.S. Hudson, J. Kuhn, J. McCormack, G. North, W. Sprigg, S.T. Wu (Eds.), Solar Variability and Its Effects on Climate. Geophysical Monograph 141, American Geophysical Union, 2004, pp. 171–193.